BUREAU OF MINERAL RESOURCES, GEOLOGY AND GEOPHYSICS

REPORT 247

BMR MICROFORM 196

DOWN-HOLE TEM RESPONSE IN THE PRESENCE OF A CONDUCTIVE OVERBURDEN

by

J.A. MAJOR

DEPARTMENT OF RESOURCES AND ENERGY

Minister: Senator the Hon. Peter Walsh

Secretary: A.J. Woods

BUREAU OF MINERAL RESOURCES, GEOLOGY AND GEOPHYSICS

Director: R.W.R. Rutland

ISSN 0084-7100

Published for the Bureau of Mineral Resources, Geology and Geophysics
by the Australian Government Publishing Service

CONTENTS

FIGURES

ABSTRACT

Model studies were made to provide a suite of curves illustrating the transient electromagnetic (TEM) response down drillholes through a conductive overburden into a resistive host, and through a conductive overburden overlying a conductive prism approximating the Elura orebody. The results show that at early sample times the overburden alone generates the near-surface signal. At depth the response of the orebody is complicated: it may add to or subtract from the overburden response, depending on the sample time and the transmitter-receiver and orebody geometry. Separate tests with the orebody in electrical contact with the overburden and with the orebody insulated from it indicate, for this simple model, that there is only a marginal increase in the orebody response when it is in contact with the overburden. Comparison of the model curves with field observations obtained from SIROTEM down-hole surveys at Elura enable the bulk resistivity of the overburden and orebody to be determined.

1. INTRODUCTION

A series of down-hole transient electromagnetic (TEM) scale-model studies was carried out on a part-time basis between May and December 1980 by the Bureau of Mineral Resources (BMR) to provide a suite of curves illustrating the down-hole TEM response of a vertical rectangular prism beneath a conductive overburden. The model suite approximates the situation at the Elura deposit. Hence the model studies can be compared with field observations made at Elura by Hone & Pik (1980). The main motivation behind this modelling work was to verify some of the findings of Hone & Pik (1980) in their down-hole TEM fieldwork at Elura.

For further information on the TEM method the reader is referred to Velikin & Bulgakov (1967) and Spies (1980).

2. THEORY OF EM SCALE MODELLING

The general theory of EM scale modelling, starting from Maxwell's equations and introducing the constraints of linearity and time invariance, is described by Sinclair (1948). The application of modelling to EM problems in geophysics is presented by Ward (1967); Spies (1980) gives the scaling relationships for TEM modelling. The requirements for the model to simulate the field situation are:

$$\mu_m = \mu \qquad (1)$$

$$\sigma_m L_m^2/T_m = \sigma L^2/T \qquad (2)$$

$$V_m/V = L_m T/LT_m \qquad (3)$$

where the subscripted variables are the model parameters and the unsubscripted variables are the field parameters, and

μ is magnetic permeability (H/m)

σ is conductivity (S/m)

T is time (s)

L is length (m)

V is electric potential (V)

3. DESCRIPTION OF THE MODEL AND EXPERIMENTAL SET UP

The measurements were made on the Macquarie University TEM modelling facility, which has been described by Spies (1979). The model parameters and loop specifications are given in Appendix 1. Appendix 2 discusses the calibration and frequency response of the receiver coil and its effect on the TEM measurements.

A typical experimental set up is shown in Figure 1. The overburden was modelled by a graphite slab, and the orebody by a block of type metal. One series of measurements was made with the type metal electrically insulated from the graphite (by a computer card 0.18 mm thick), and another series was made with the type metal bonded to the graphite by conductive epoxy resin.

4. PRESENTATION OF RESULTS

As described in Appendix 3 the model results and field results of Hone & Pik (1980) were normalised for the turns-area product of the receiver coils, and are plotted in units of microvolts per amp per turn per square metre.

Figure 2 is a pictorial index of the models showing the relative positions of the transmitter loop, borehole, and orebody either in plan or in section. Appropriate field results from Elura are shown as dashed lines in Figures 3 to 21 for a particular borehole-Tx loop configuration irrespective of the position of the orebody.

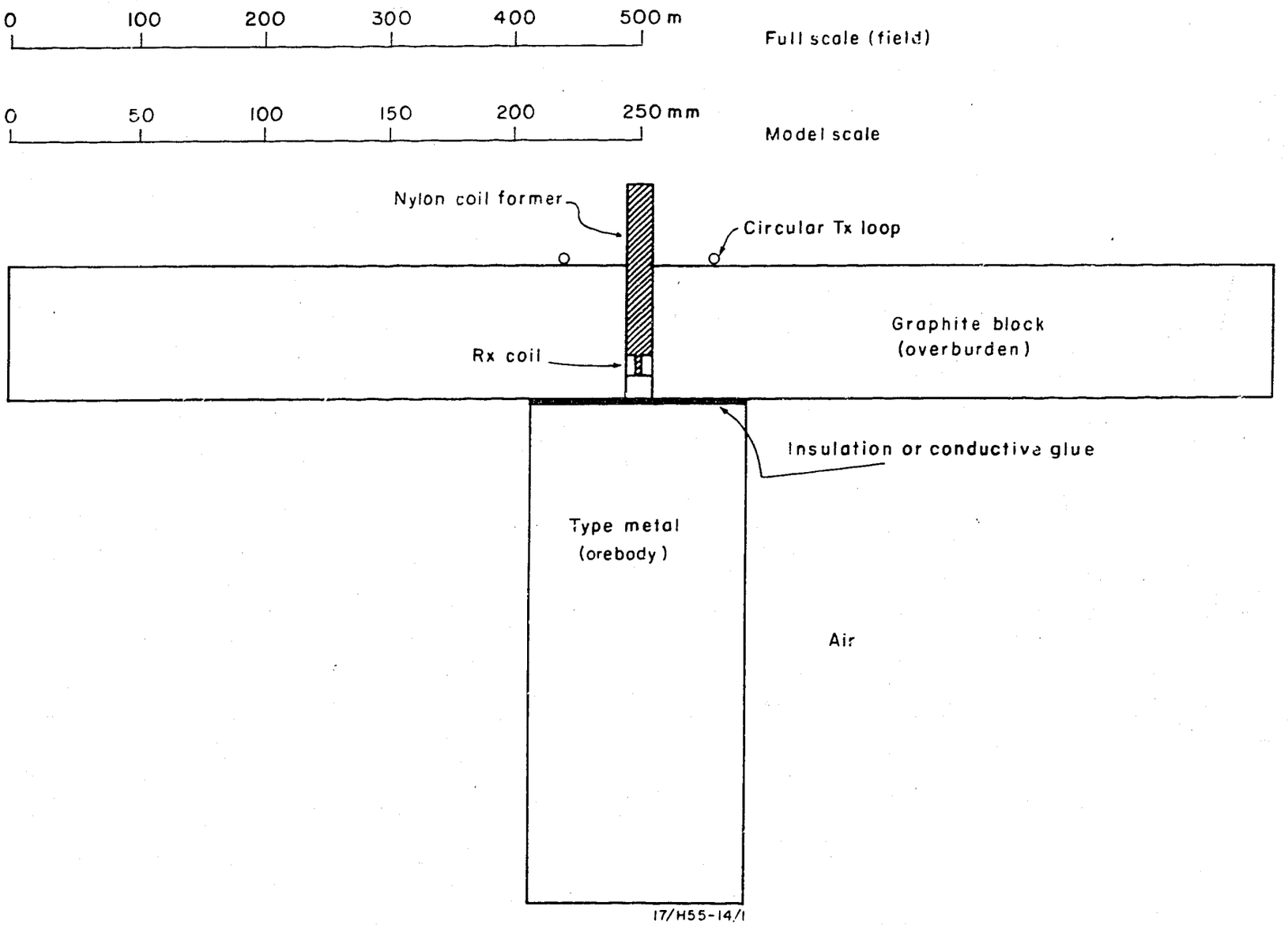

Fig. 1 Typical experimental set up: cross-section of Elura model beneath conductive overburden.

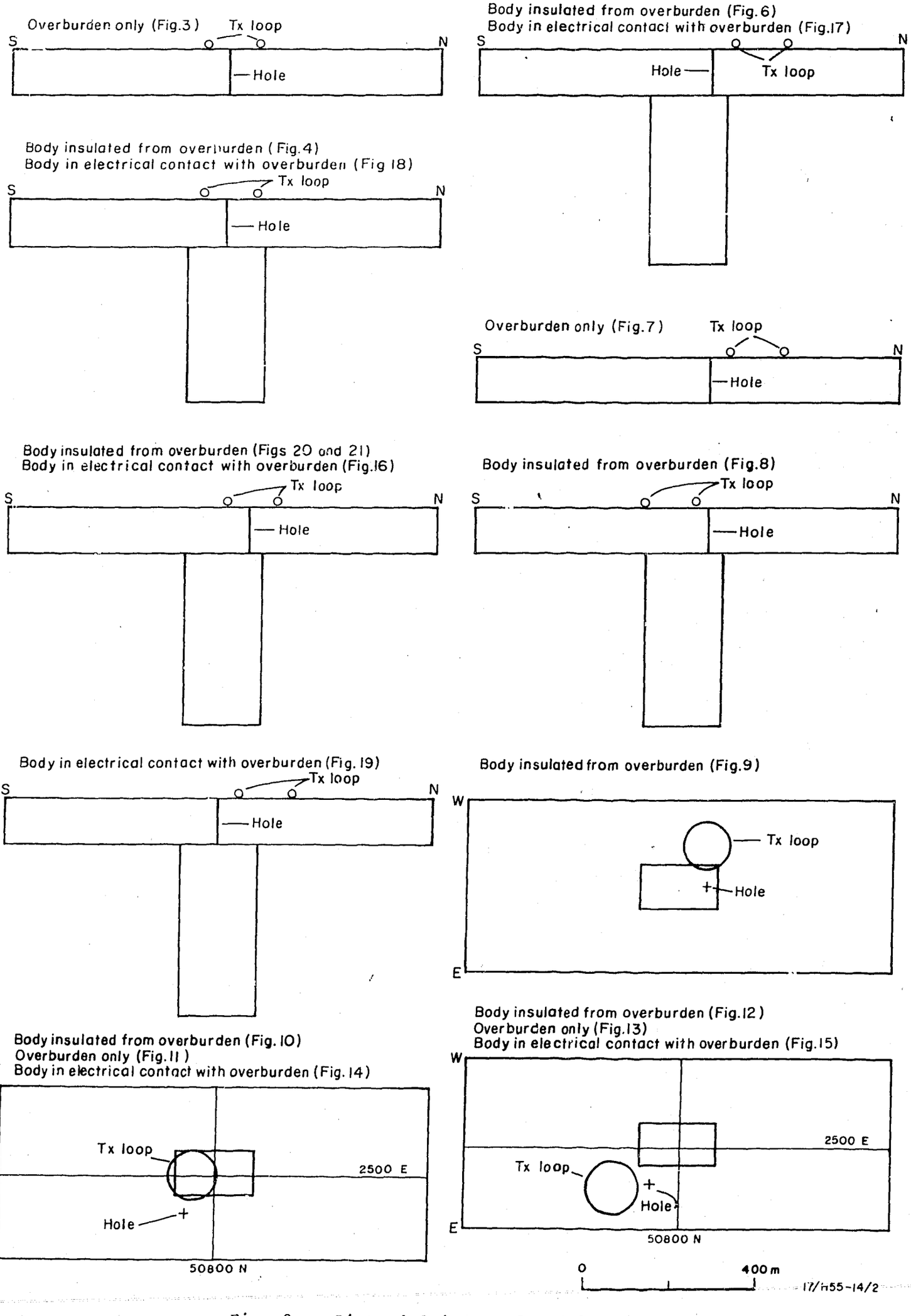

Fig. 2 Pictorial index of models.

5. COMPARISON OF MODEL RESULTS

In this section no reference is made to the field results.

Overburden only

Figure 3 shows that for the overburden alone, the signal increases with depth down to 60 or 70 m in the time range 0.76 to 2.4 ms. Below 70 m the signal decreases steadily with depth. At 4 ms there is no pronounced increase in the signal with depth, and it appears to remain fairly uniform irrespective of depth. These phenomena can be explained qualitatively using a modification proposed by Hone & Pik (1980) of the equivalent current filament or 'smoke ring' concept of Nabighian (1979). In Hone & Pik's (1980) model of the conductive overburden, a closed current filament of decreasing strength expands radially with time and is trapped in the overburden at 60-80 m depth. For a vertical TEM probe the maximum signal is observed in the plane of the current filament. Beyond 4 ms the radius of the current filament is so large that the signal strength is virtually independent of depth within the range of observations (5 to 120 m).

Borehole and transmitter loop centred on orebody

Comparison of Figures 3 and 4 shows that the orebody has no effect on the response at 0.76 ms, all of which can be attributed to the overburden. Beyond 1.6 ms the orebody contributes to the signal even at the surface, and by 4 ms the total signal at the surface is 3 times that of the overburden alone.

Figure 4 shows that from 1.6 to 8.3 ms there is a monotonic increase in signal strength with depth down to the top of the orebody. The increase is less pronounced at later sample times. A possible explanation of the decreased slope of the curves is that at early sample times the dominant

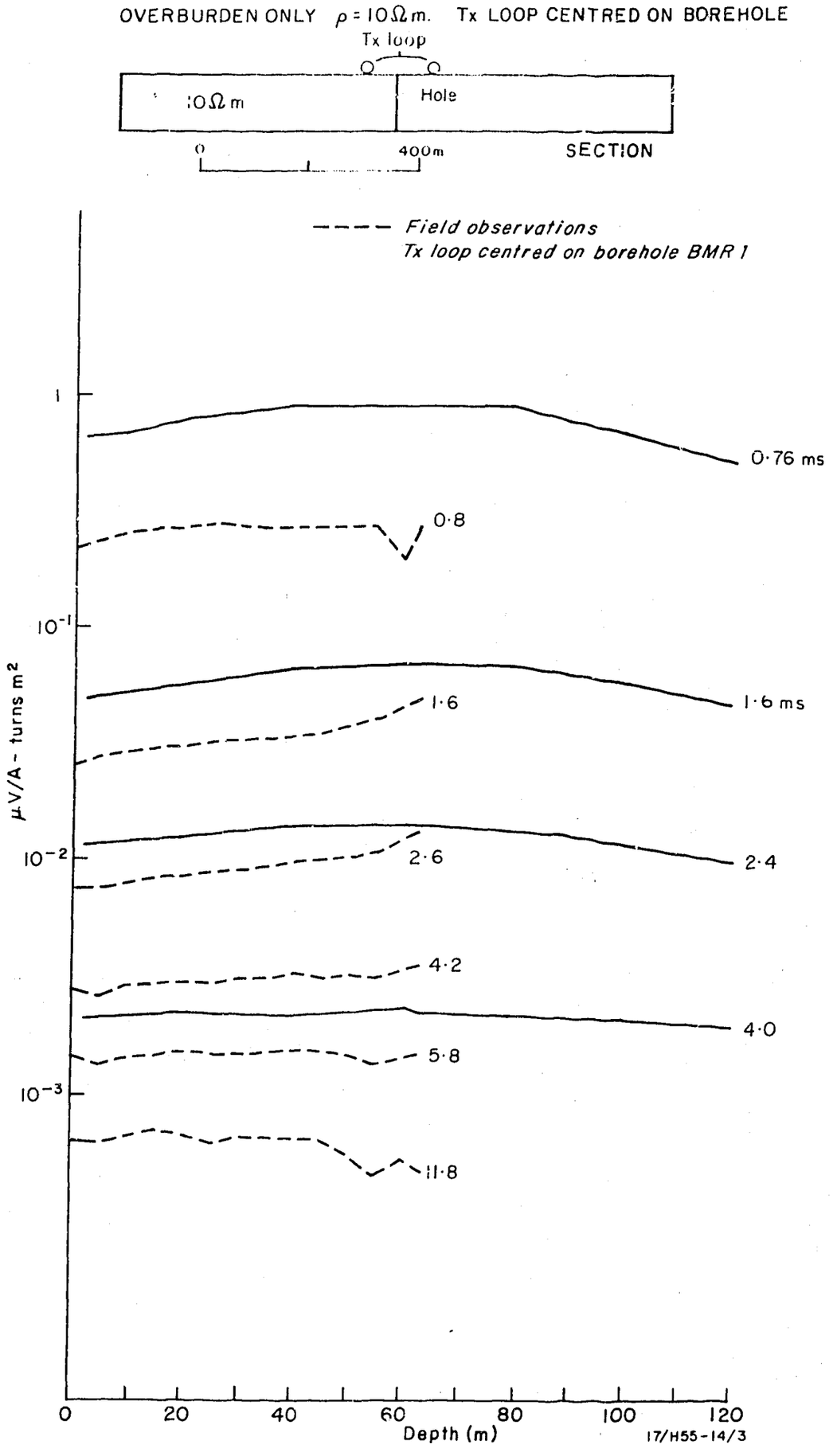

Fig. 3 Overburden only. Transmitter loop centred on borehole.

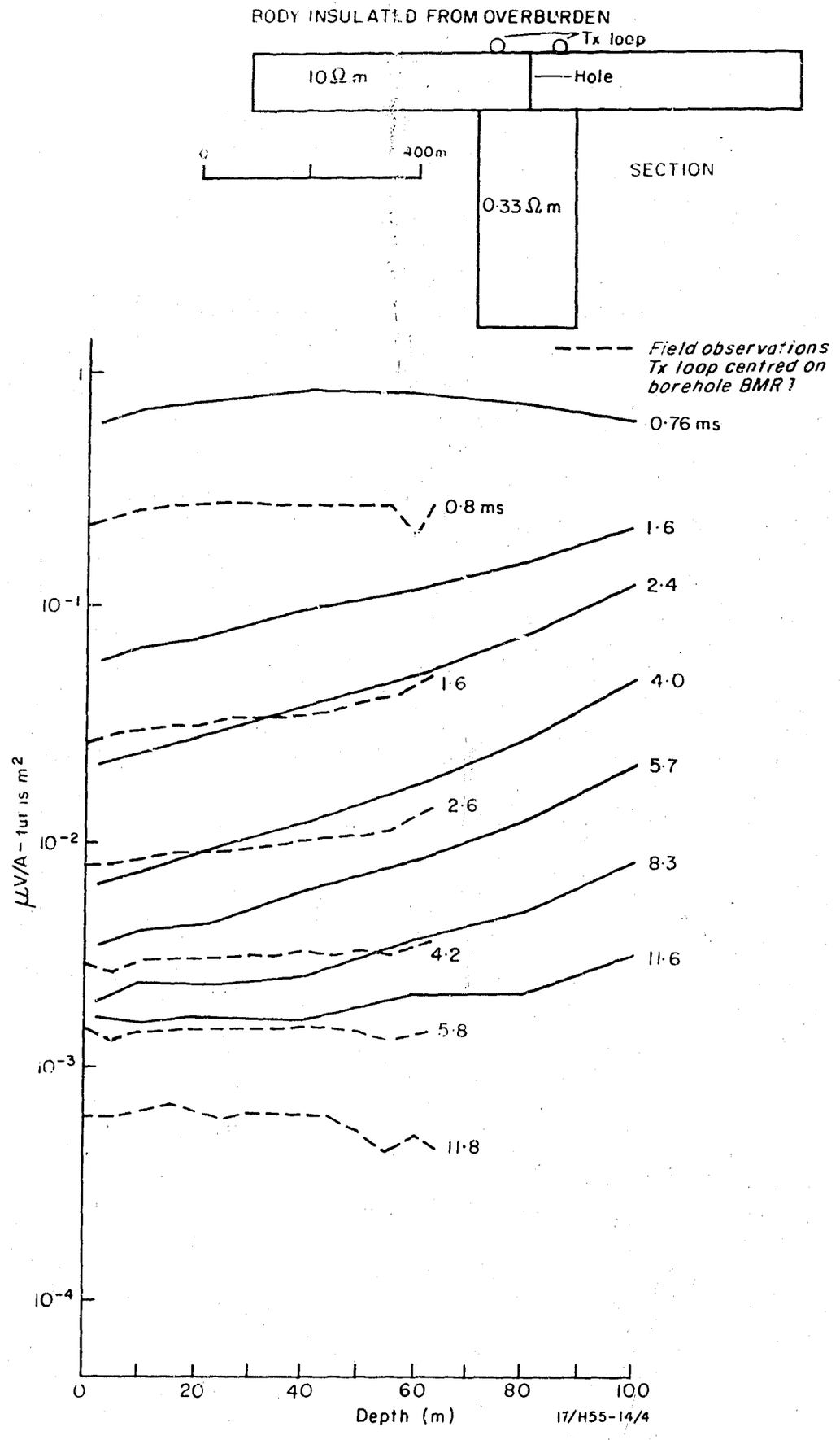

Fig. 4 Borehole and transmitter loop centred on orebody. Body insulated from overburden.

eddy current flow is near the upper surface of the orebody, so that an increase in depth of a few metres produces a large proportional change in the signal strength. At late sample times the eddy currents have diffused deep down and into the body, so that the same increase in depth makes a smaller proportional change in the response.

Comparison of Figures 4 and 18 shows there is only a slight enhancement (1.3 times) of the signals at 1.6 and 2.4 ms when the orebody is in electrical contact with the overburden. Beyond 4 ms it makes little difference whether or not the orebody is in contact with the overburden. Only a small difference at early sample times is to be expected in a model with horizontal boundaries in which the dominant induced current flow is horizontal. There is only a small component of current flow normal to the boundary, and hence it is unimportant whether the boundary is a conductor or insulator. If there are boundaries normal to the dominant induced current flow, as there are for the Elura orebody, then the electrical conductivity at the boundaries will be important and would affect the TEM results significantly. To check this suggestion, a more elaborate model could be constructed in which the upper surface of the body penetrates the overburden for a distance corresponding to some tens of metres in the field.

Borehole near north end of orebody; transmitter loop centred on borehole

Comparison of Figures 4 and 5 shows a drop in response from the orebody when the transmitter and receiver are moved from the centre of the body to a point 30 m south of the northern end. From the model results there is little evidence for the category C response (an increase at early sample times and a decrease at late sample times) predicted by Hone & Pik (1980).

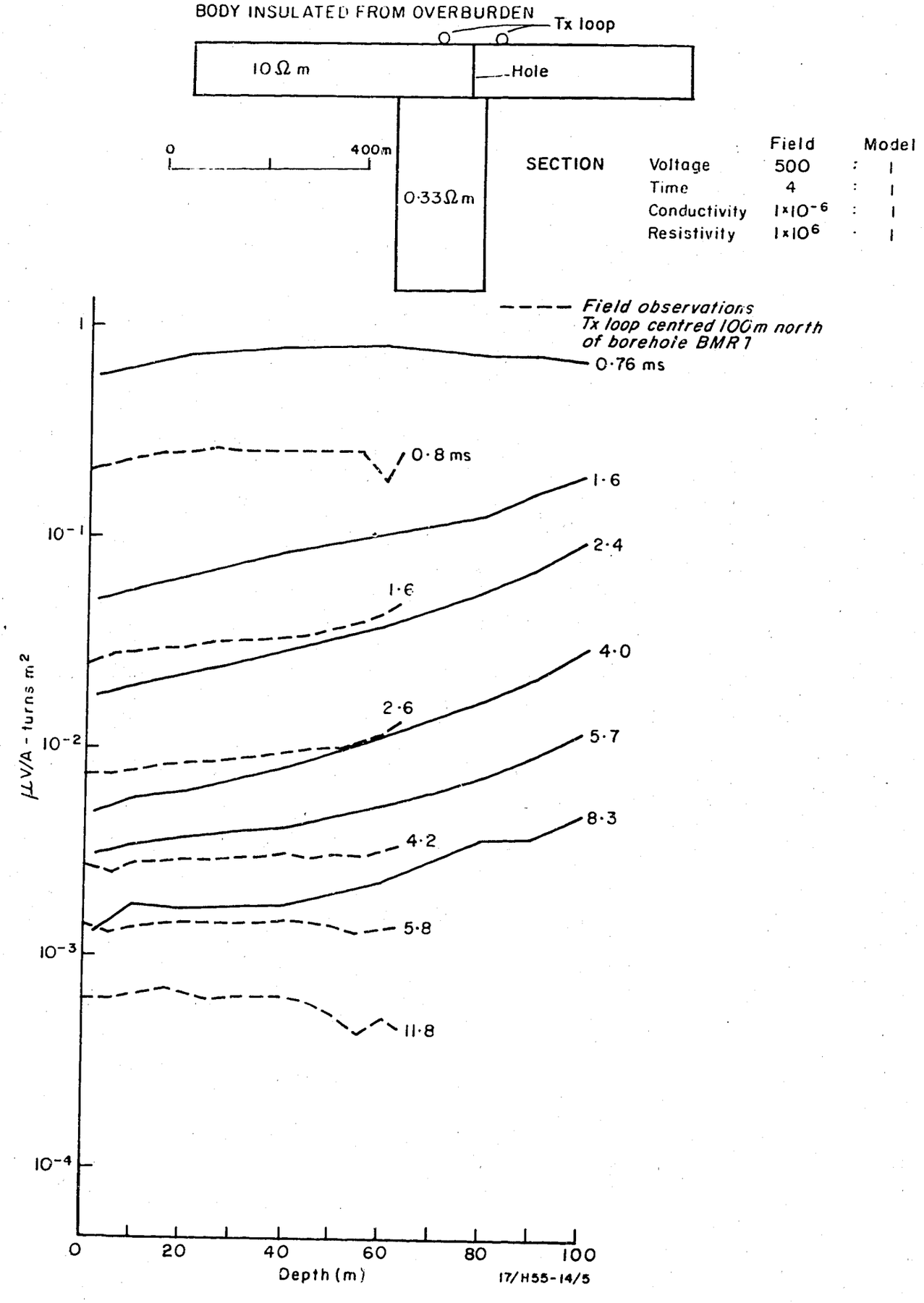

Fig. 5 Borehole 30 m south of north end of orebody. Transmitter loop centred on borehole. Body insulated from overburden.

Comparison of Figures 5 and 16 shows again only a slight enhancement in response (1.4 times at 20 m for delays of 1.6 and 2.4 ms) when the orebody is in electrical contact with the overburden.

Borehole near north end of orebody; transmitter loop centred 100 m north of borehole

Comparison of Figures 5 and 6 shows a drop in response at all sample times when the Tx loop centre is moved from the borehole to a position 100 m north. There is also a change in curve shape. For the borehole outside the loop (Fig.6) at 0.76 ms there is a sharper decrease in response with depth below 50 m, and at 1.6 ms the response increases more slowly with depth. Beyond 2.4 ms the curves are almost parallel but at a lower level than those for the loop centred on the borehole.

Comparison of Figures 6 and 7 shows that at 0.76 ms and below 50 m the decrease in respor due to the orebody is more than that due to the overburden alone, but that, at 1.6 ms and beyond, the orebody increases the response. The same features are seen in a comparison of Figures 7, and 19, where the borehole is centred on the body with the Tx loop centred 100 m north of the borehole. These features cannot be explained adequately in terms of eddy currents in the overburden and orebody; however, it is worth noting that coincident-loop surface TEM model results for a resistive layer over a conductive halfspace also show a decrease in signal strength at early sample times, followed by an increase at late sample times (see Raiche & Spies, 1981).

Comparison of Figures 6 and 17 shows that a conductive contact between the overburden and orebody slightly enhances the orebody response

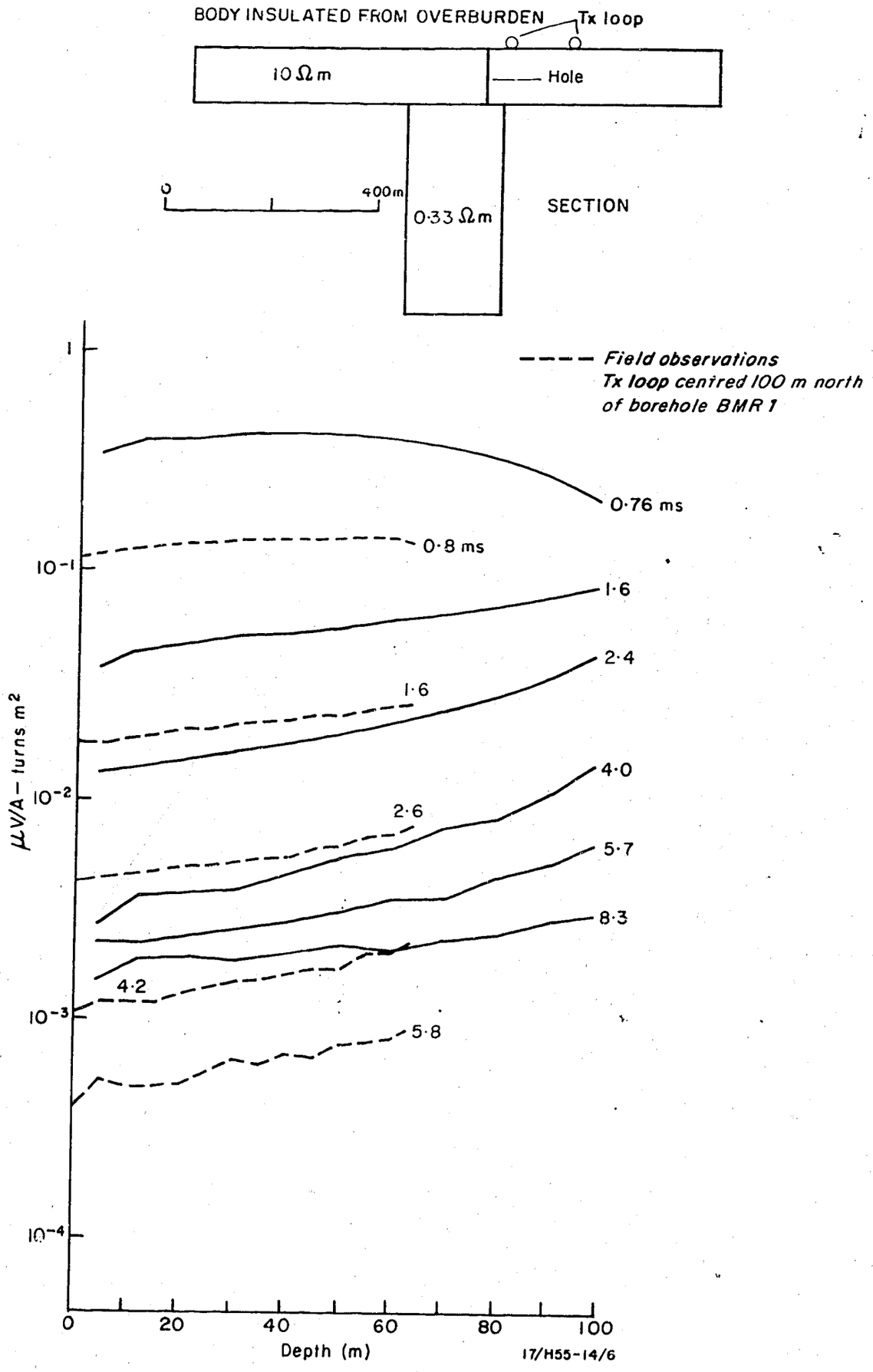

Fig. 6 Borehole 30 m south of north end of orebody. Transmitter loop centred 100 m north of borehole. Body insulated from overburden.

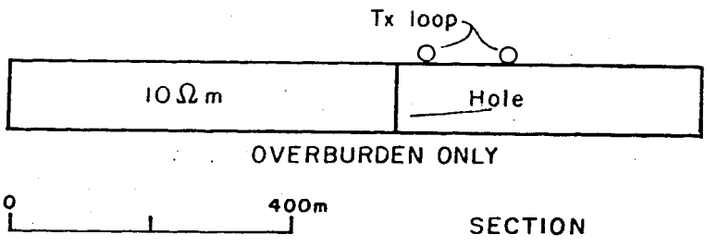

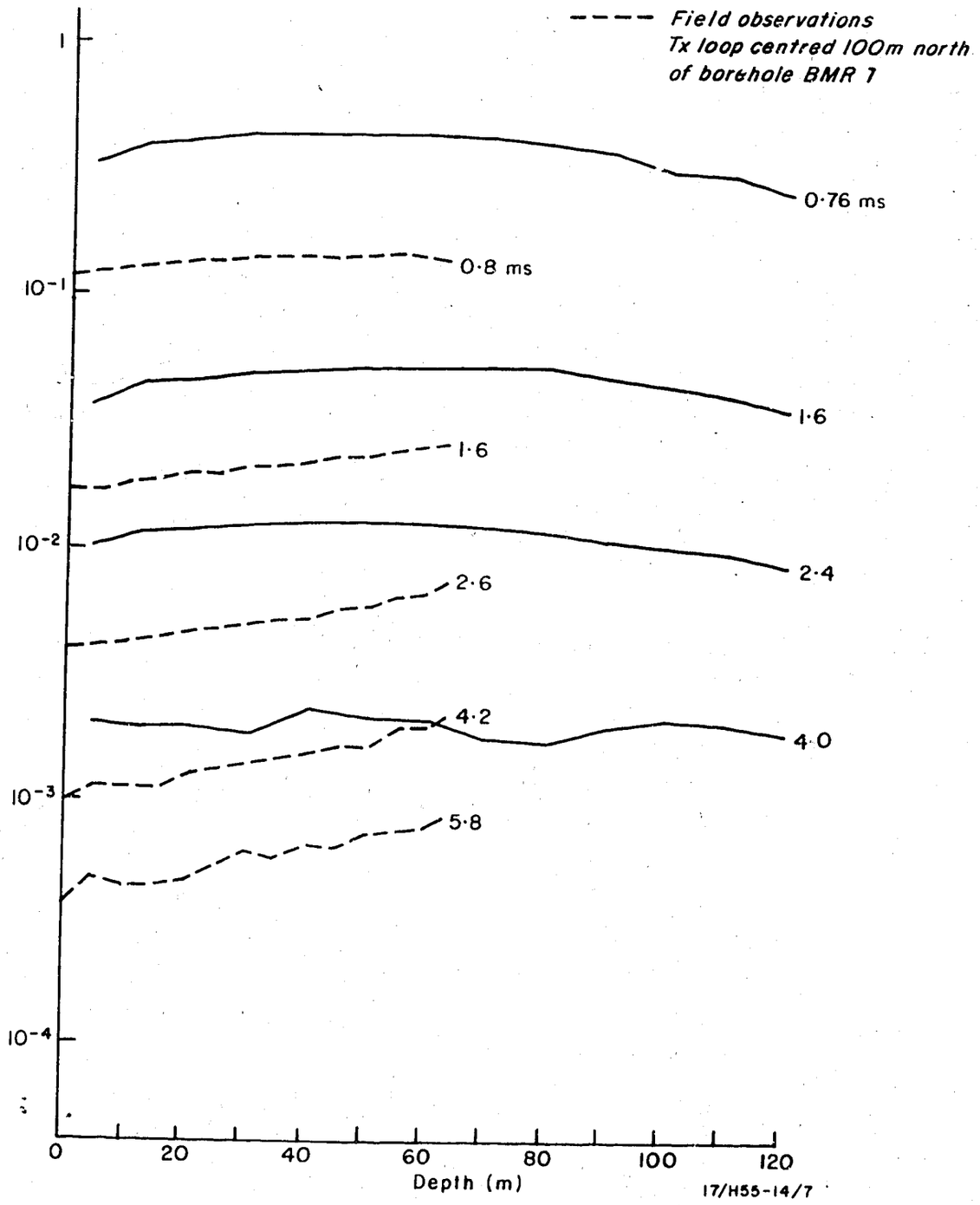

Fig. 7 Overburden only. Transmitter loop centred 100 m north of borehole.

from 1.6 to 4 ms, but, at 5.7 ms and beyond, the conductivity of the contact is immaterial possibly because the eddy currents are then concentrated deep within the orebody and away from the contact.

Borehole near north end of orebody; transmitter loop centred 100 m south of borehole

Comparison of Figures 8 and 6 shows that at the early sample times of 0.76 and 1.6 ms it makes little difference whether the Tx loop is over the main bulk of the body or off one end. Figure 8 shows a decrease in signal strength from that of the overburden only (Fig. 7) with depth at 0.76 ms, and shows an increase with depth at later times. At 2.4 ms and beyond, the signals are stronger (particularly near the surface) with the loop over the bulk of the body (Fig. 8) than with the loop off one end (Fig. 6).

Borehole near north end of orebody; transmitter loop centred 100 m west of borehole

Figures 9 and 6, in which the Tx loop is west and north of the body respectively, show a similar response except at 0.76 ms. With the Tx loop west of the body the response at 0.76 ms is less than the response with the Tx loop north of the body over the entire depth range. This cannot be explained adequately in terms of the orebody and overburden configuration because other experiments (Figs. 3 and 4) showed the body to have no effect at 0.76 ms on the surface readings. The decrease may be due to the proximity of the western edge of the graphite slab to the transmitter loop, so that the overburden no longer approximates an infinite layer.

Measurements in hole off the orebody; transmitter loop centred over southern part of orebody

In this model the hole is located 90 m from the orebody in a position approximating the shaft at Elura.

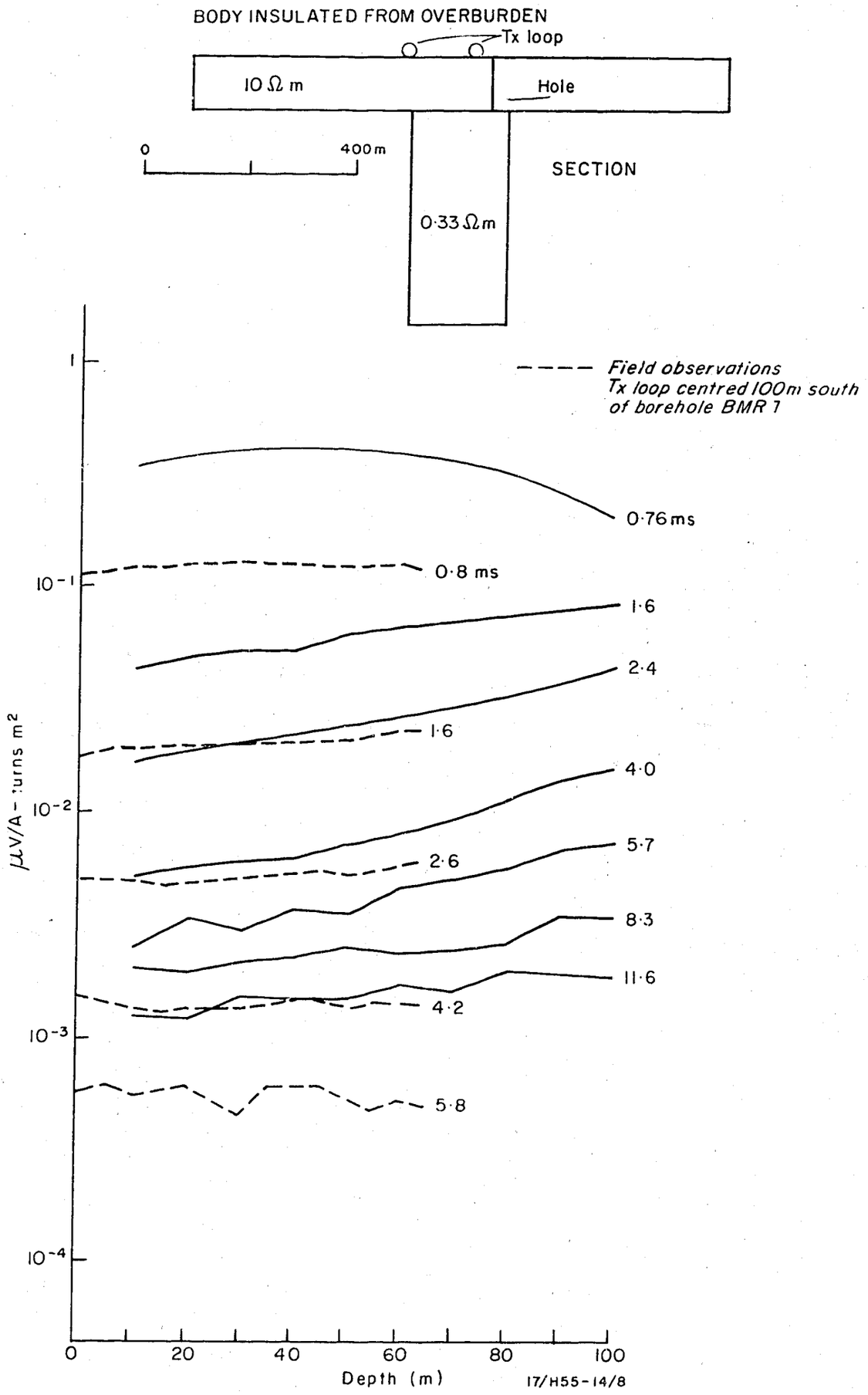

Fig. 8 Borehole about 30 m south of north end of orebody. Transmitter loop centred 100 m south of borehole. Body insulated from overburden.

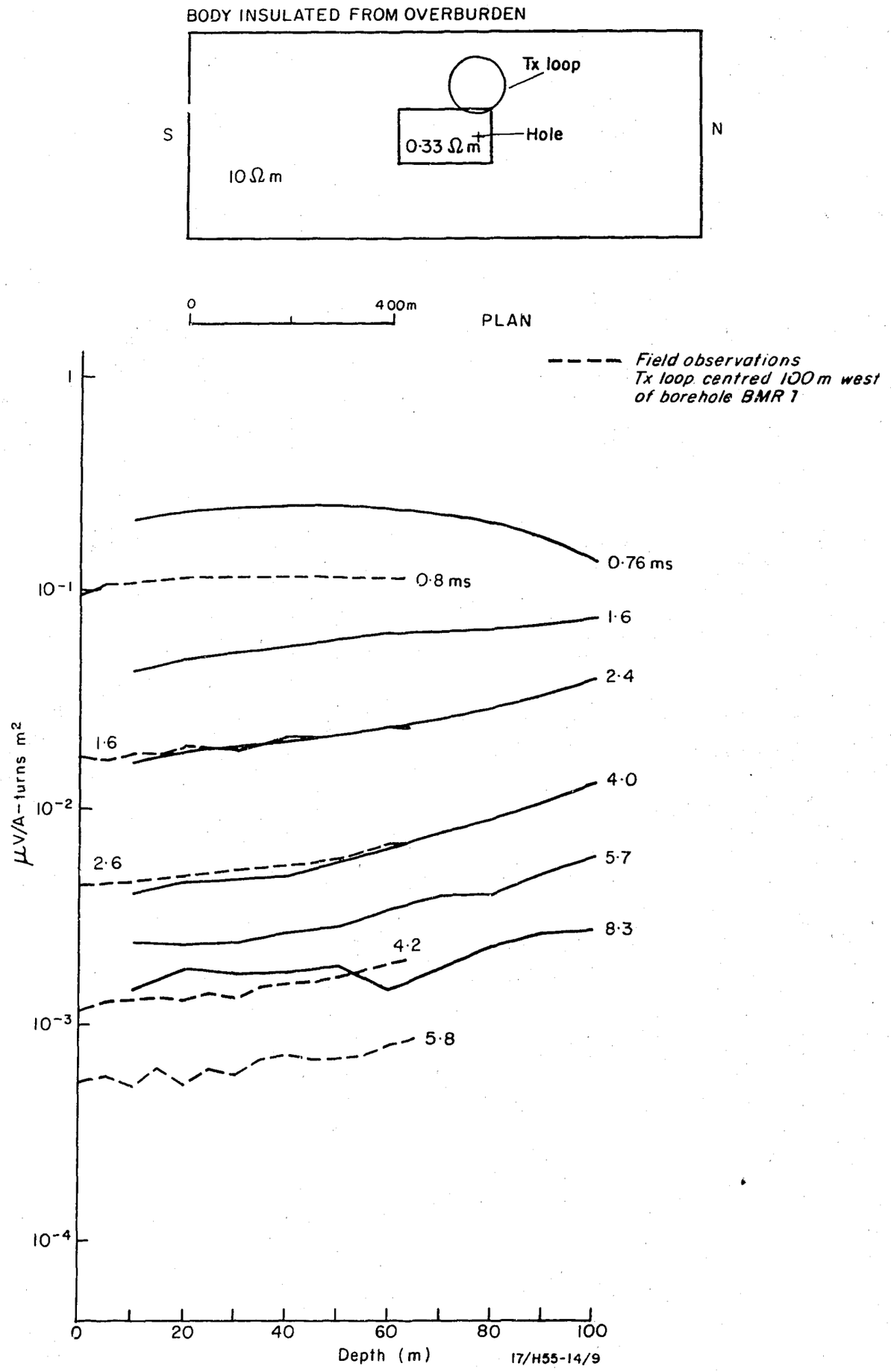

Fig. 9 Borehole about 30 m south of north end of orebody. Transmitter loop centred 100 m west of borehole. Body insulated from overburden.

Comparison of Figures 10 and 11 shows that at 0.76 ms the response measured in the hole is due to the overburden alone. At 1.6 and 2.4 ms more than 70 m deep the orebody decreases the response below that of the overburden alone. At 4 ms there is a slight increase in the response above that of the overburden down to 90 m, and below 90 m there is a decrease with negative readings at 150, 160, and 170 m. Below 170 m the response again becomes positive.

Comparison of Figures 10 and 14 shows that the response observed in the hole is virtually independent of electrical contact at the orebody-overburden boundary.

Measurements in hole off the orebody; transmitter loop not over orebody

In this model the hole again is in a position approximating the Elura shaft.

Comparison of Figures 12 and 13 shows that with the exception of a slightly enhanced signal at 4 ms there is no recognisable response from the orebody. This enhanced signal at 4 ms would be impossible to detect in the field as the increase is only 1.4 and the shapes of both logs are much the same; it may even be due to experimental error.

Figures 12 and 15 show almost identical results irrespective of electrical contact at the orebody-overburden boundary. So again, even with the orebody in electrical contact with the overburden it would not be detected in the hole with the Tx loop off the body in the position shown.

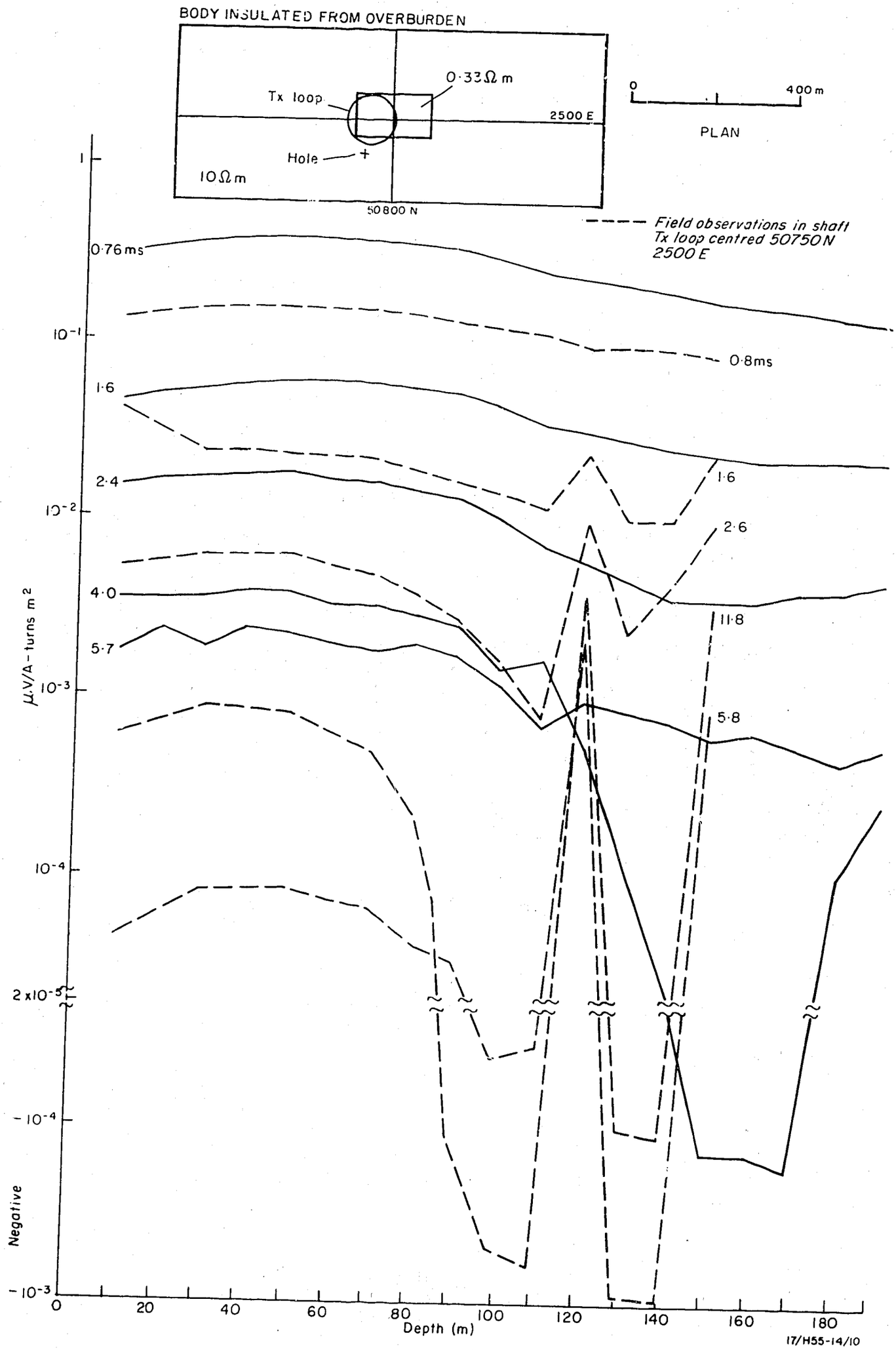

Fig. 10 Measurements in hole approximating position of Elura shaft. Transmitter loop centred 50750N 2500E 90 m from hole. Body insulated from overburden.

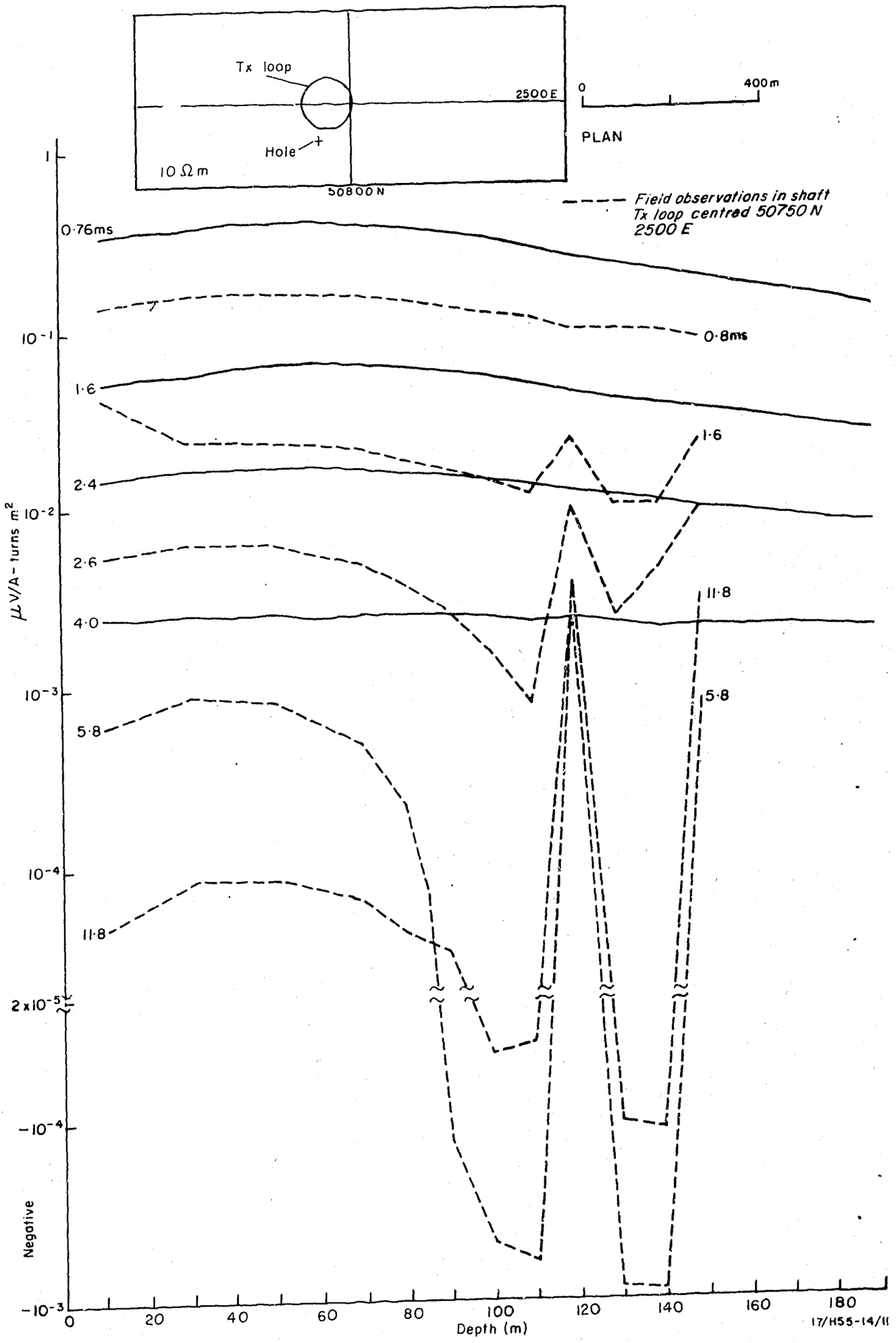

Fig. 11 Measurements in hole approximating position of Elura shaft. Transmitter loop centred 50750N 2500E 90 m from hole. Overburden only.

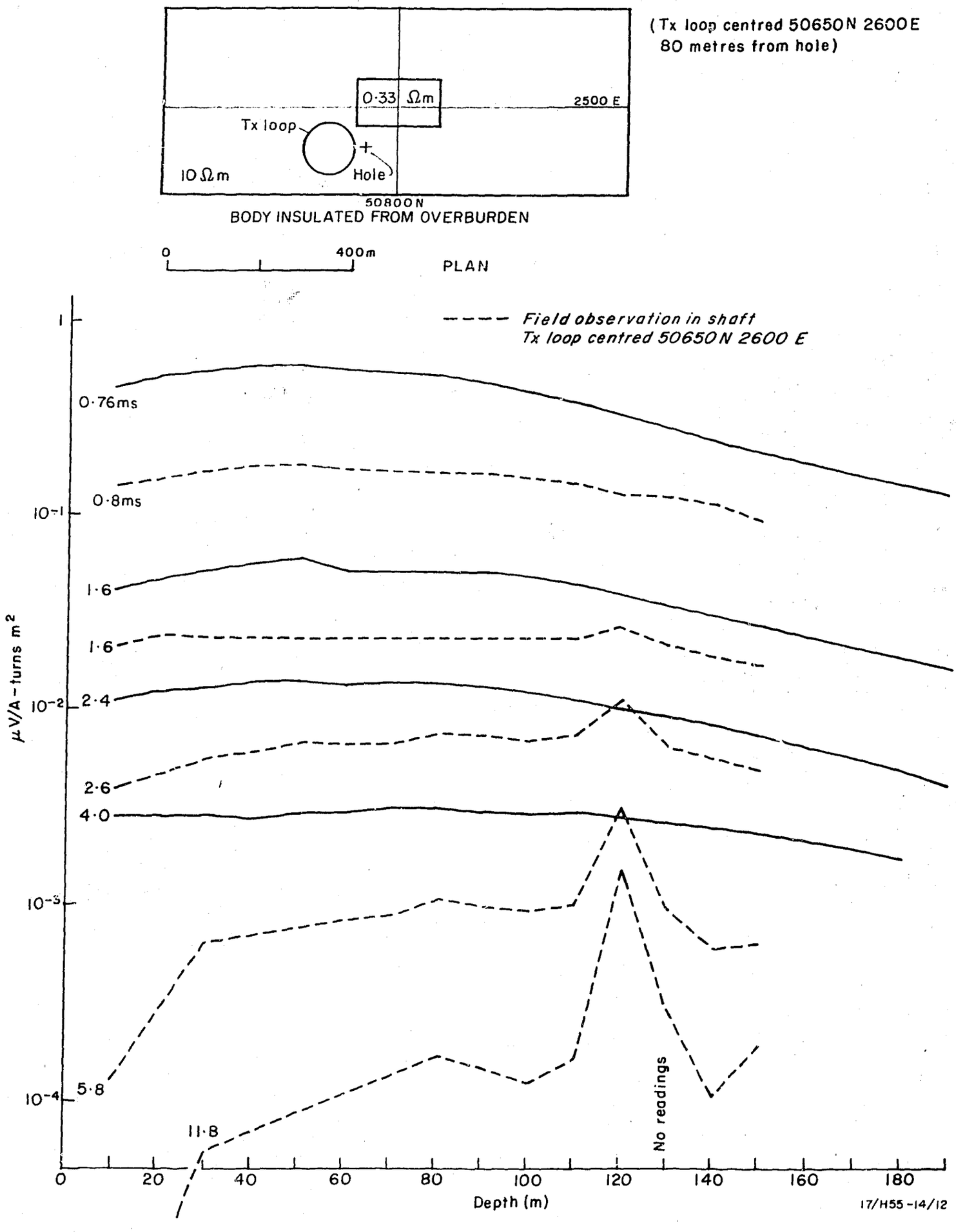

Fig. 12 Measurements in hole approximating position of Elura shaft. Transmitter loop centred 50650N 2600E 80 m from hole. Body insulated from overburden.

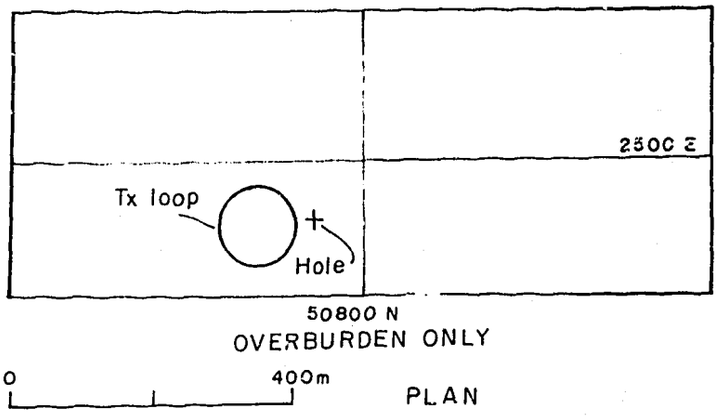

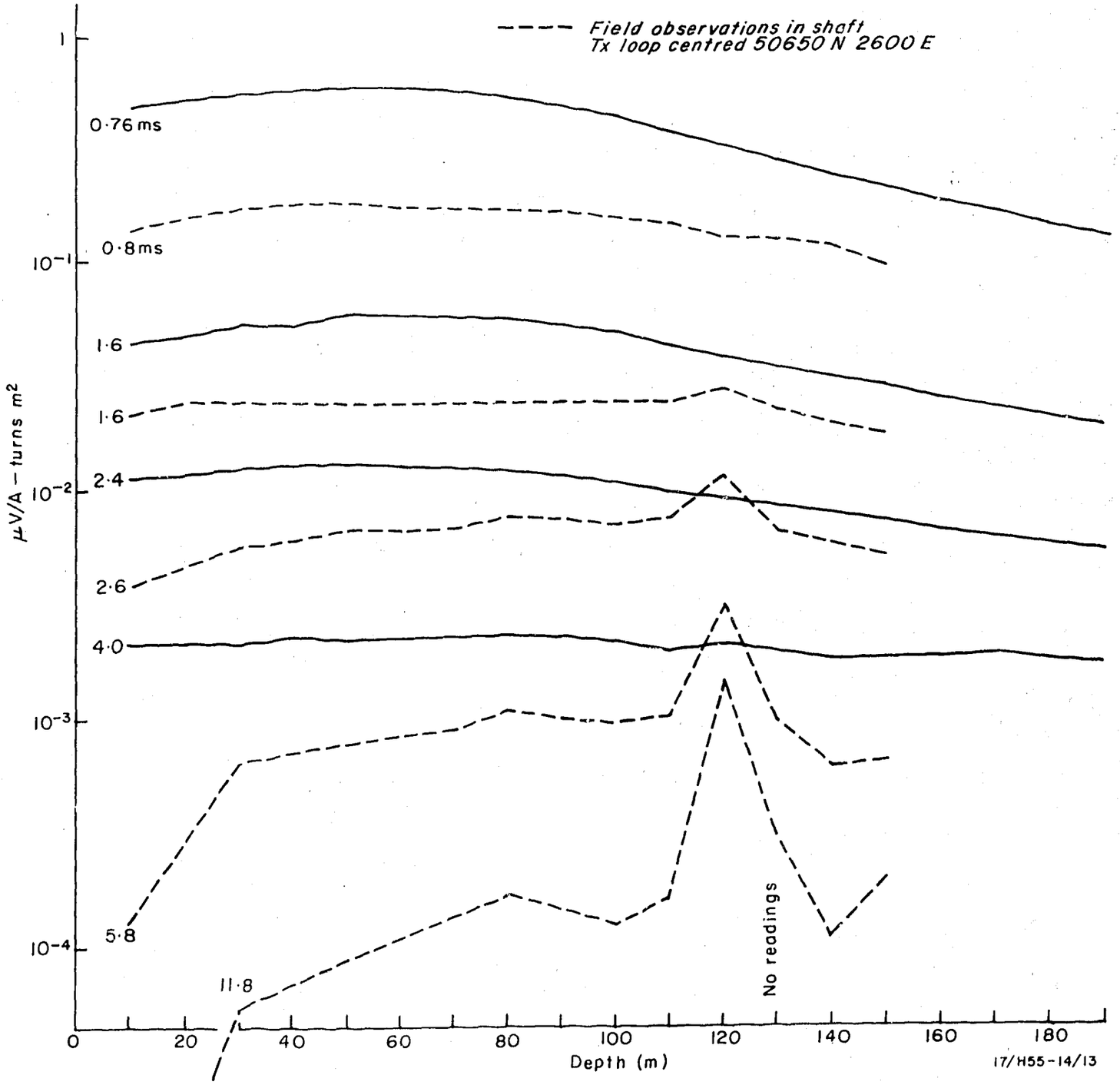

Fig. 13 Measurements in hole approximating position of Elura shaft. Transmitter loop centred 50650N 2600E 80 m from hole. Overburden only.

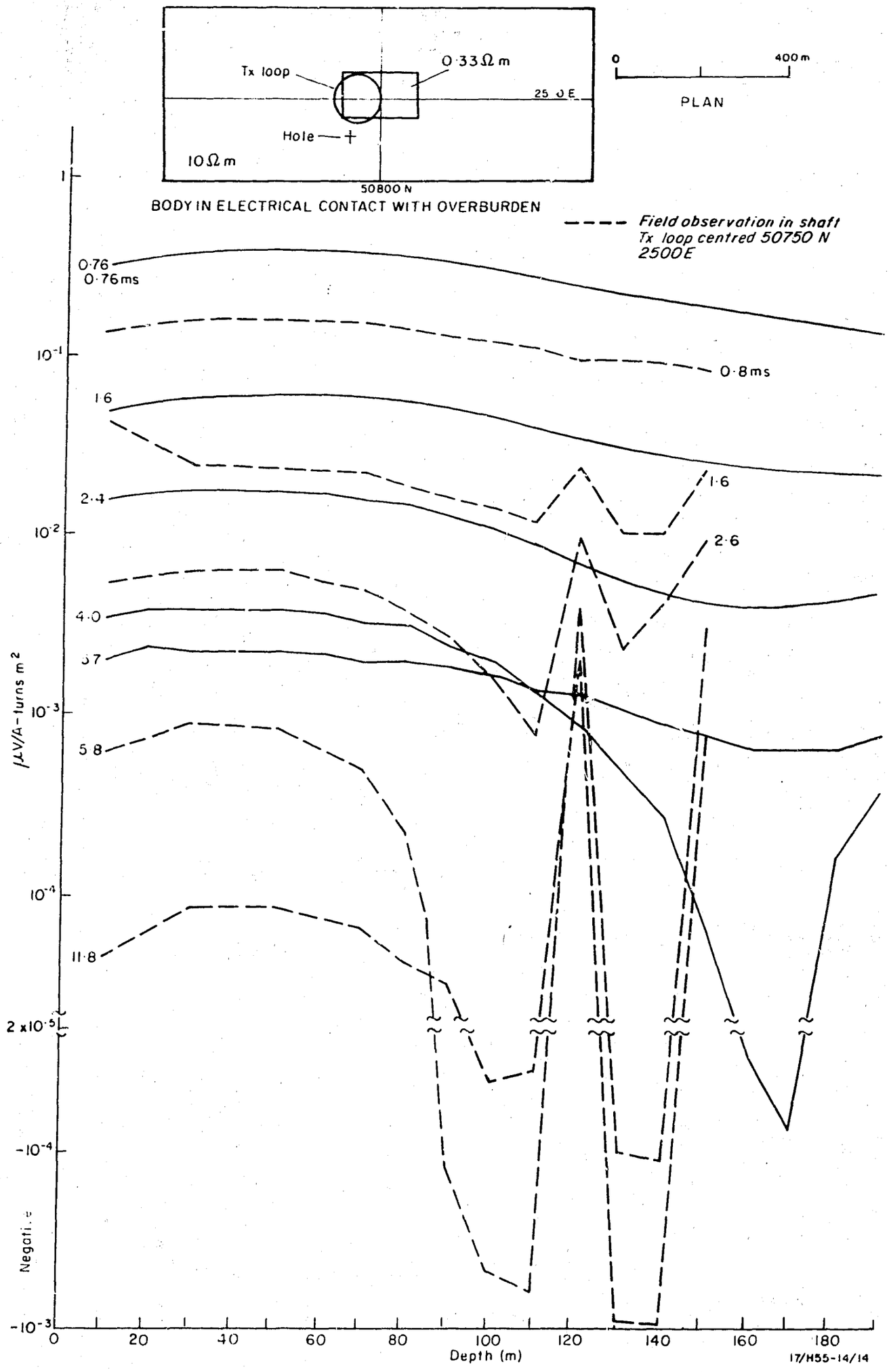

Fig. 14 Measurements in hole approximating position of Elura shaft. Transmitter loop centred 50750N 2500E 90 m from hole. Body in electrical contact with overburden.

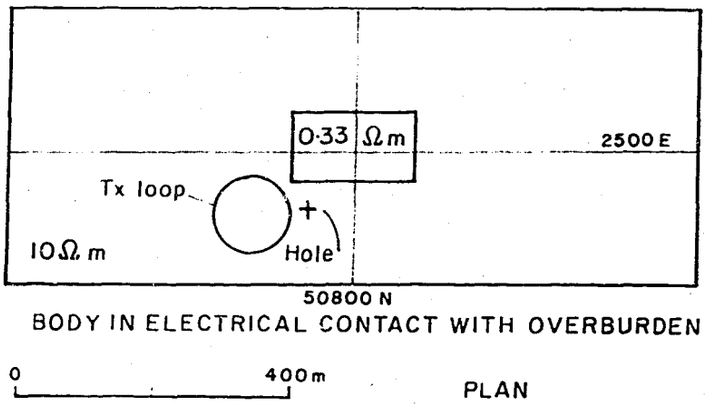

BODY IN ELECTRICAL CONTACT WITH OVERBURDEN

0 400m

PLAN

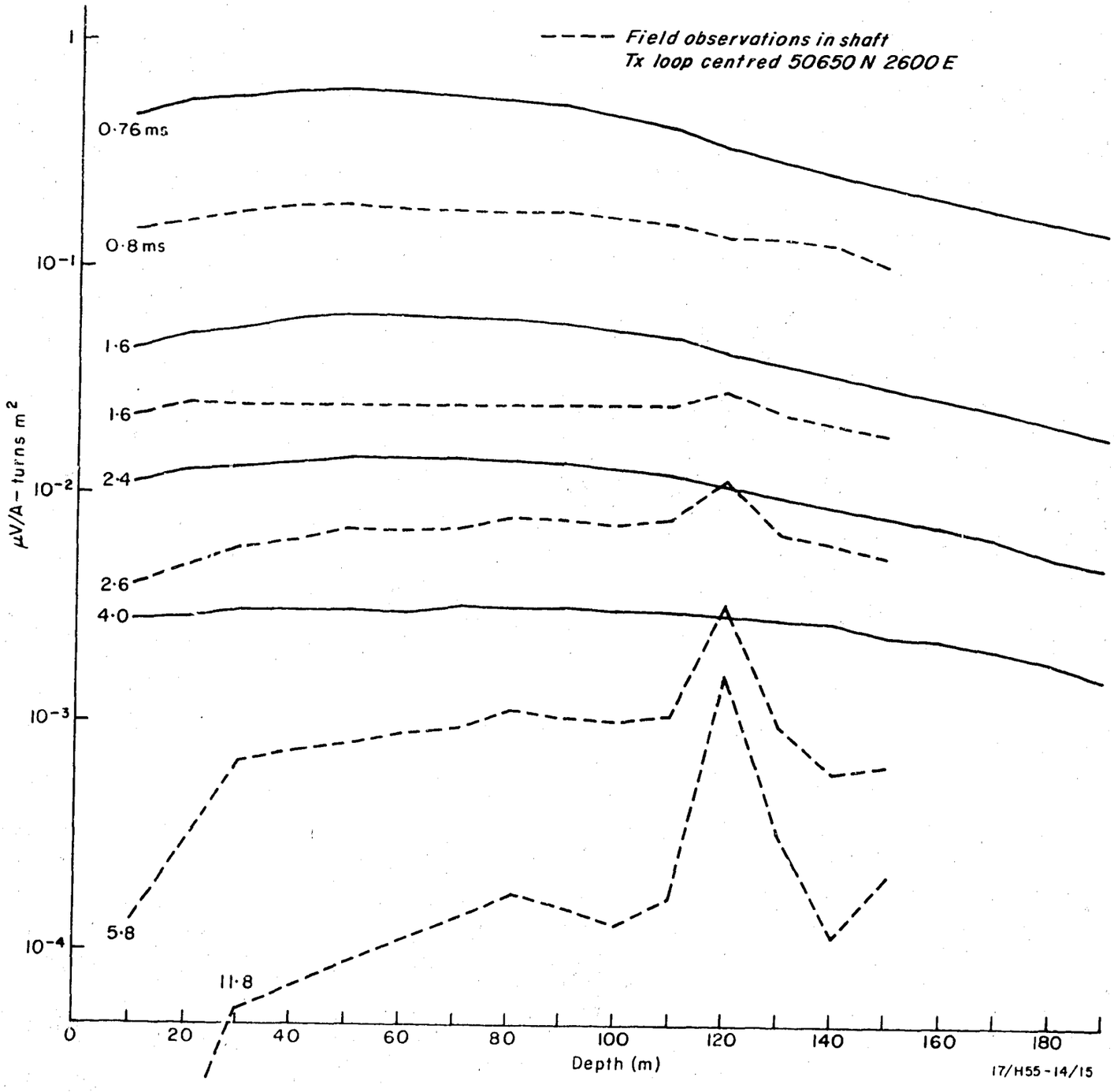

Fig. 15 Measurements in hole approximating position of Elura shaft. Transmitter loop centred 50650N 2600E 80 m from hole. Body in electrical contact with overburden.

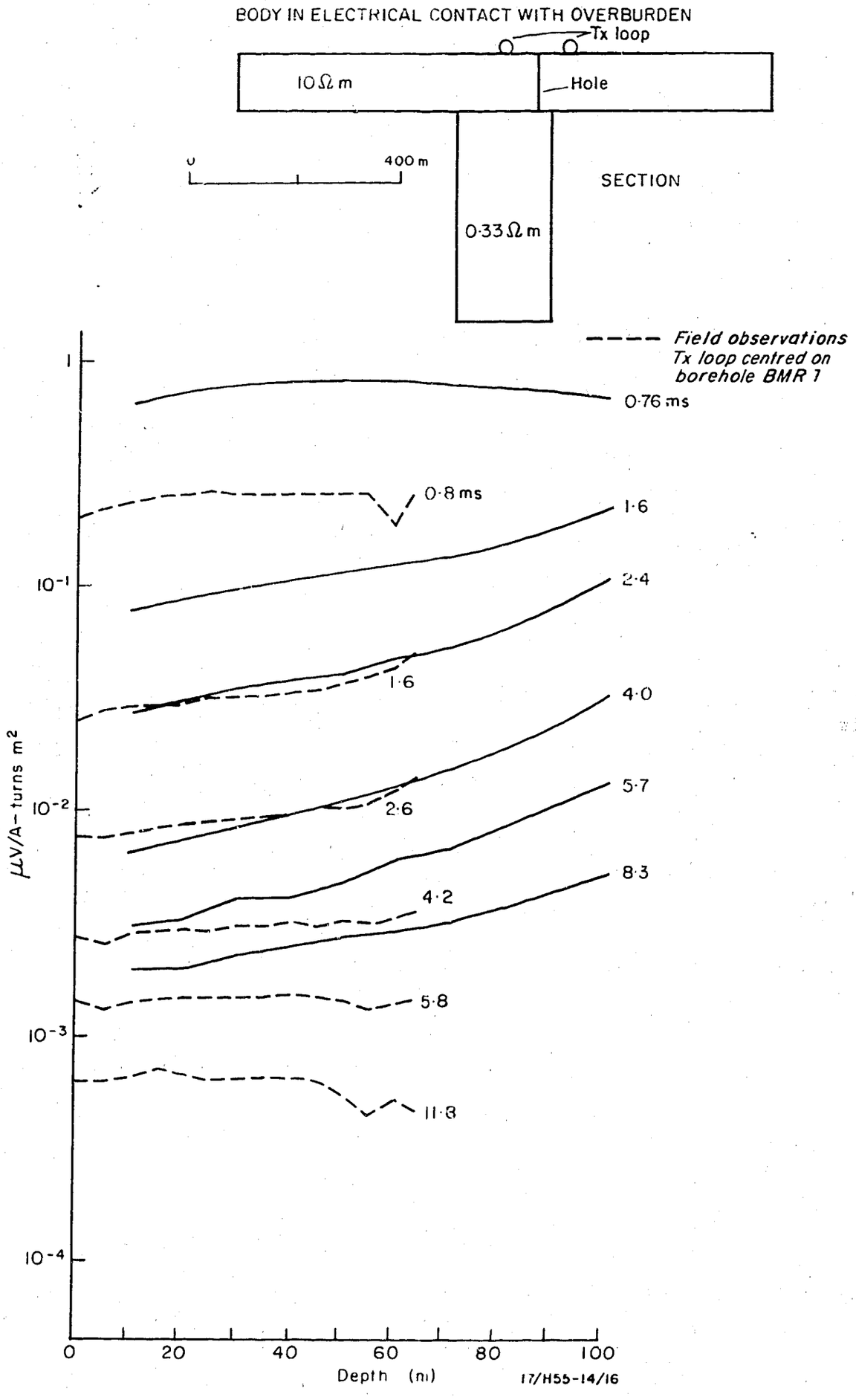

Fig. 16 Borehole 30 m south of north end of orebody. Transmitter loop centred on borehole. Body in electrical contact with overburden.

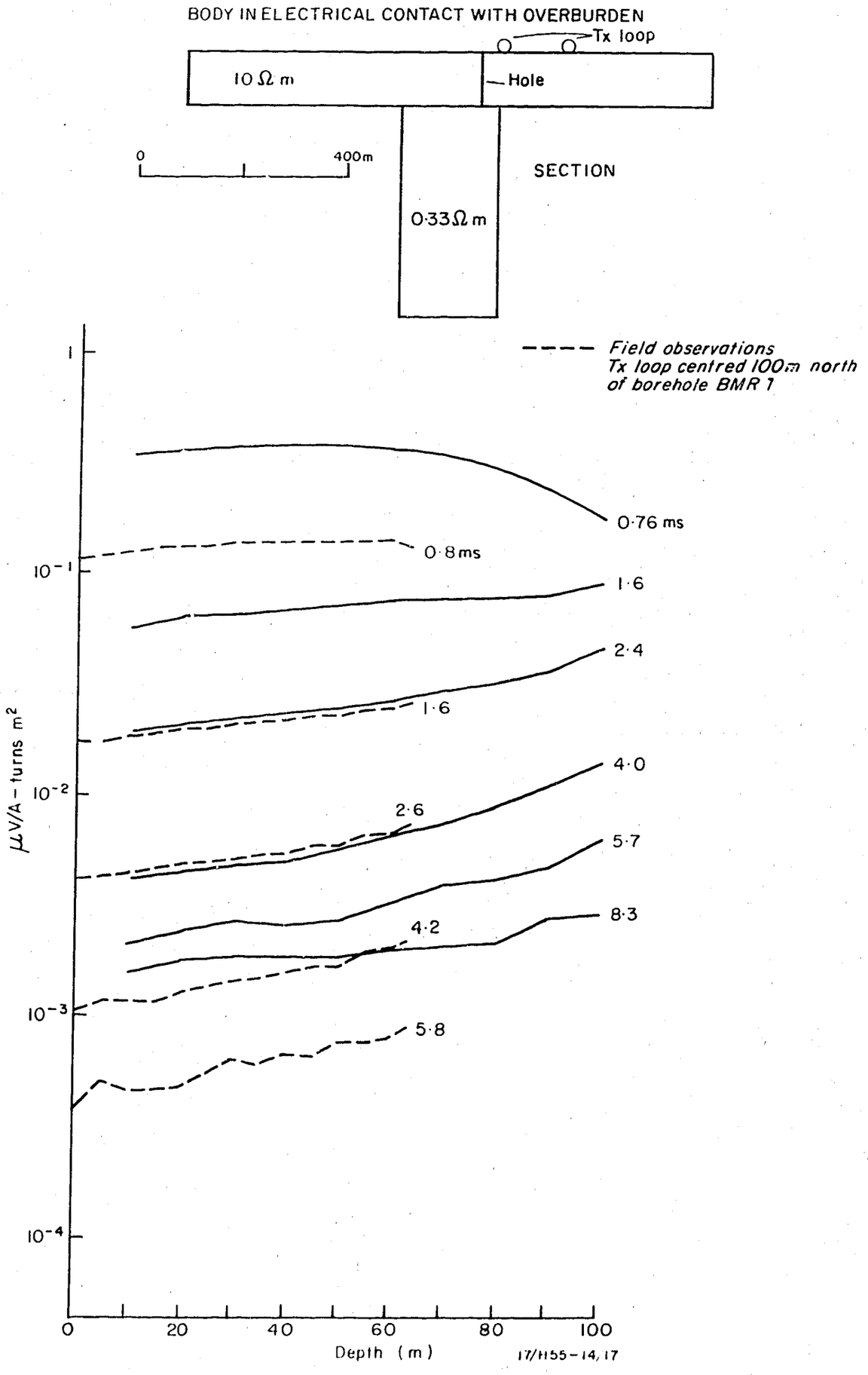

Fig. 17 Borehole 30 m south of north end of orebody. Transmitter loop centred 100 m north of borehole. Body in electrical contact with overburden.

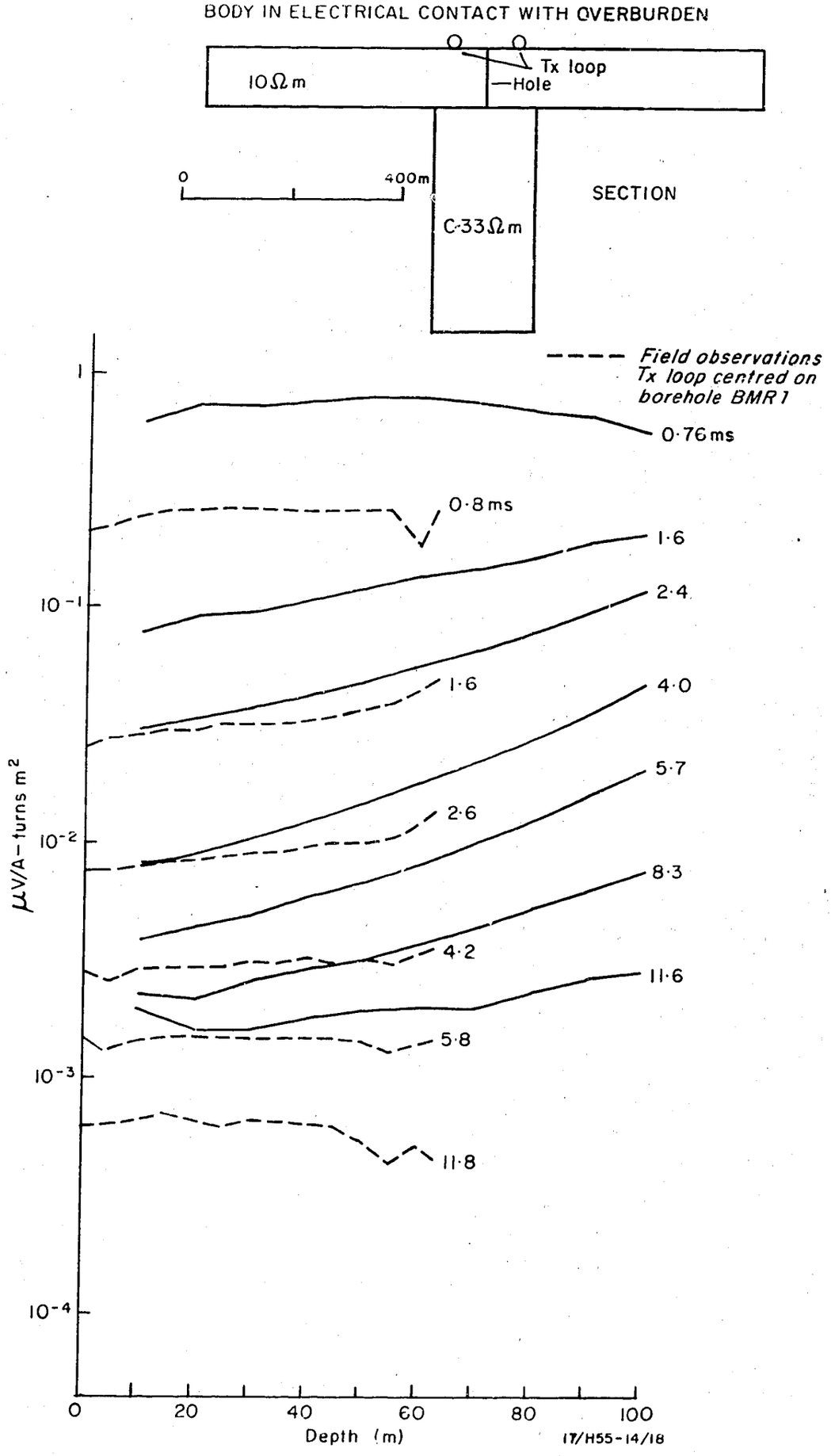

Fig. 18 Borehole and transmitter loop centred on orebody. Body in electrical contact with overburden.

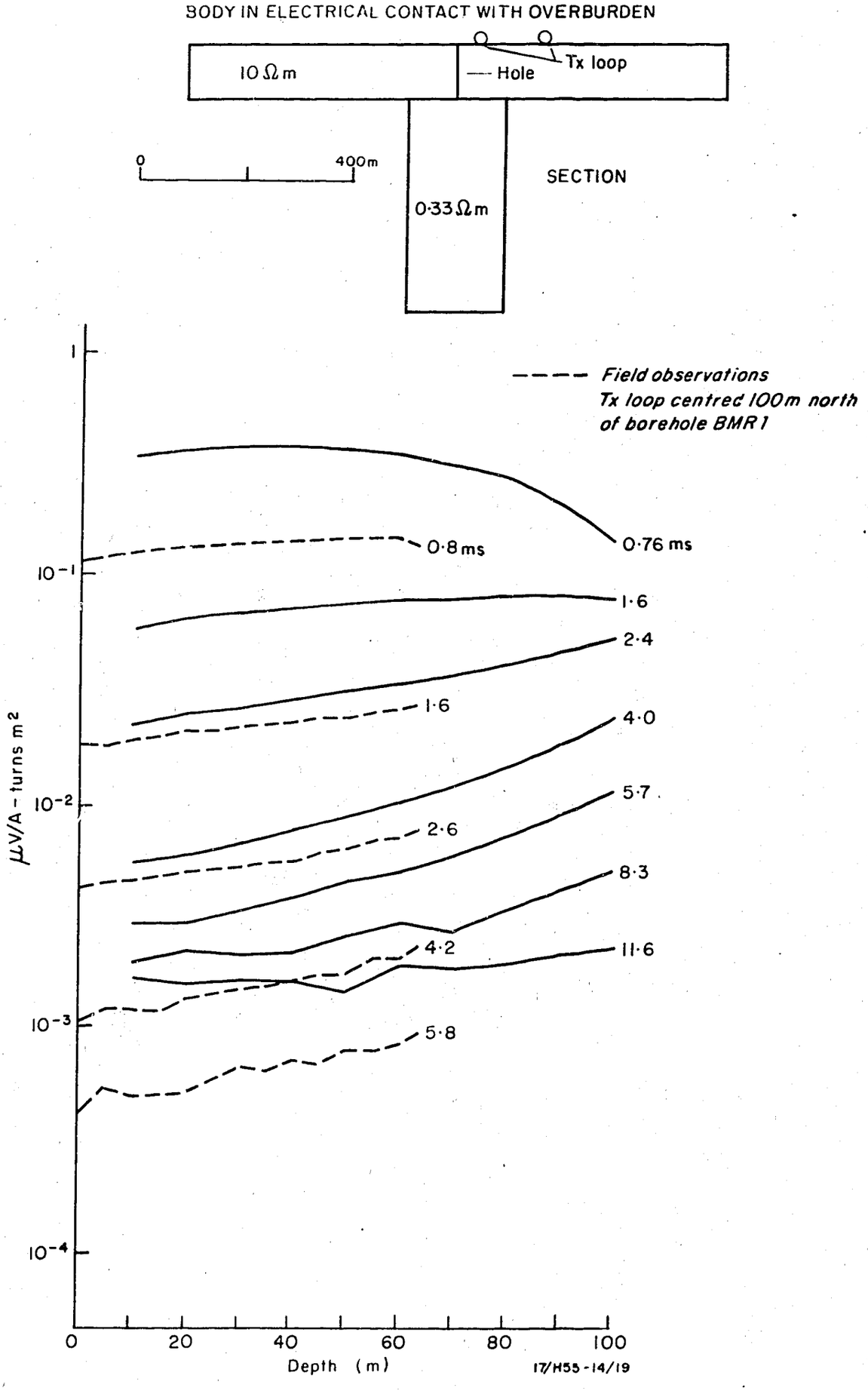

Fig. 19 Borehole centred on orebody. Transmitter loop centred 100 m north of borehole. Body in electrical contact with overburden.

6. COMPARISON OF MODEL RESULTS WITH FIELD RESULTS

When the model and field results are normalised for the turns-area product of the receiver coils (Appendix 3), the scaling relationships can be used to adjust the levels of the model curves until they match the field curves. Because the length scaling is fixed, any change in the voltage scaling implies a change in time scaling consistent with equation 3 in section 2 of this report. This in turn (because of the fixed-length scaling) implies a change in the conductivity scaling consistent with equation 2 in section 2 of this Report. Hence we can alter the voltage levels of our model curves provided that we also change the time associated with each curve, and the scaled resistivity of the model. Note that we cannot alter mathematically the ratio of the resistivities of the overburden and orebody, which is 30:1, as this is determined by the choice of model materials.

The model parameters and scaling factors of Appendix 1 were selected on the basis of available model materials and the physical property measurements of Hone (1980). These measurements gave a median value of 0.6 ohm-m for 13 samples of fresh mineralised rock and a median value of 12 ohm-m for 4 samples of weathered overburden. This is a 20:1 resistivity ratio in the field compared with 30:1 for the model, so even if the core measurements are representative of the bulk resistivities we should not expect to get a curve match for the entire time range. However, it is possible to obtain a partial curve match, which is acceptable considering the simplicity of the model compared with the complexity of the field situation.

Curve matching

The technique of curve matching is illustrated in Figures 5, 20, and 21. The normalised field observations are the dashed curves, which remain fixed. The solid curves are scaled from the model, and their level and delay time

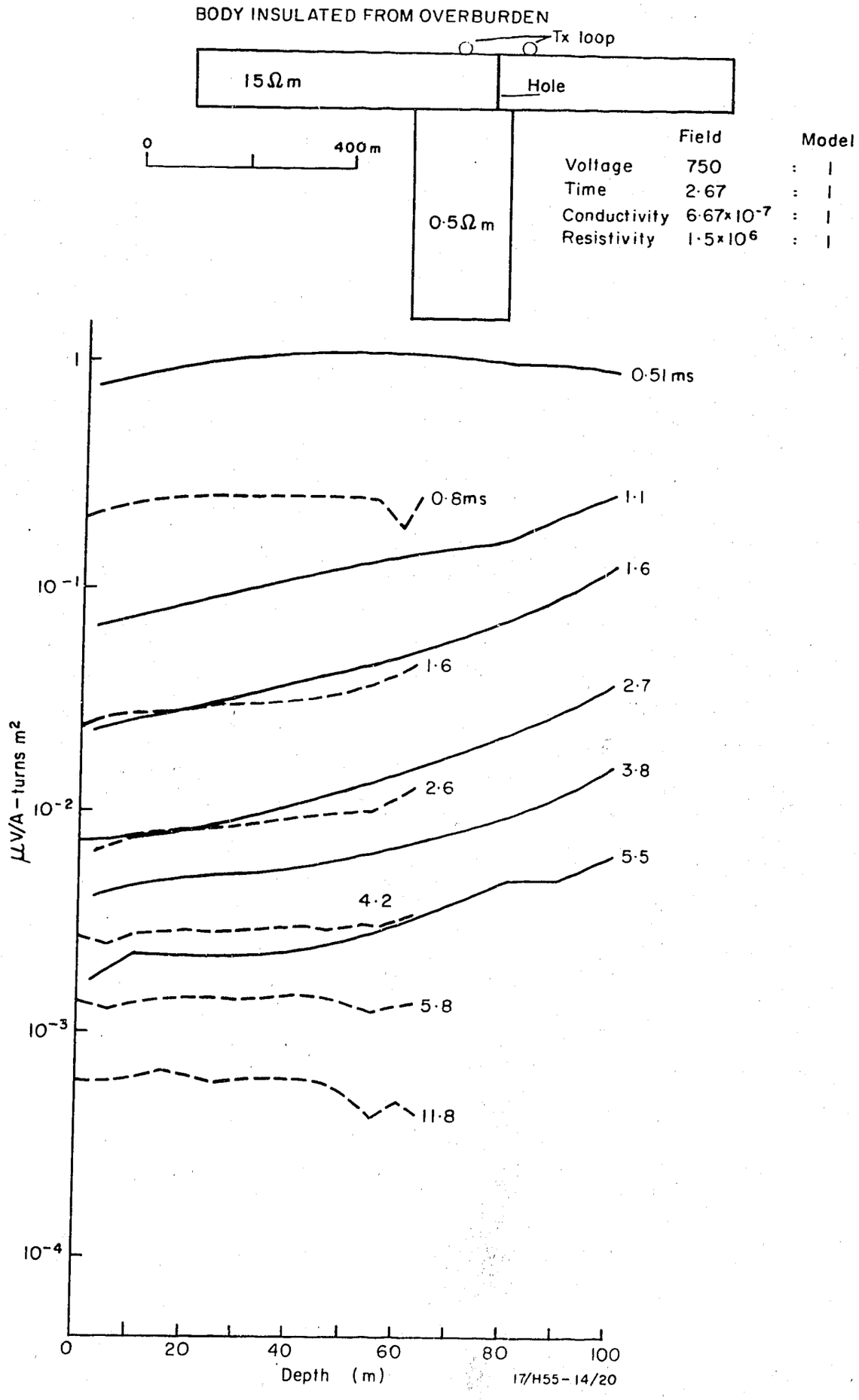

Fig. 20 Curve matching. Model as in Figures 5 and 21 but scale factors are different.

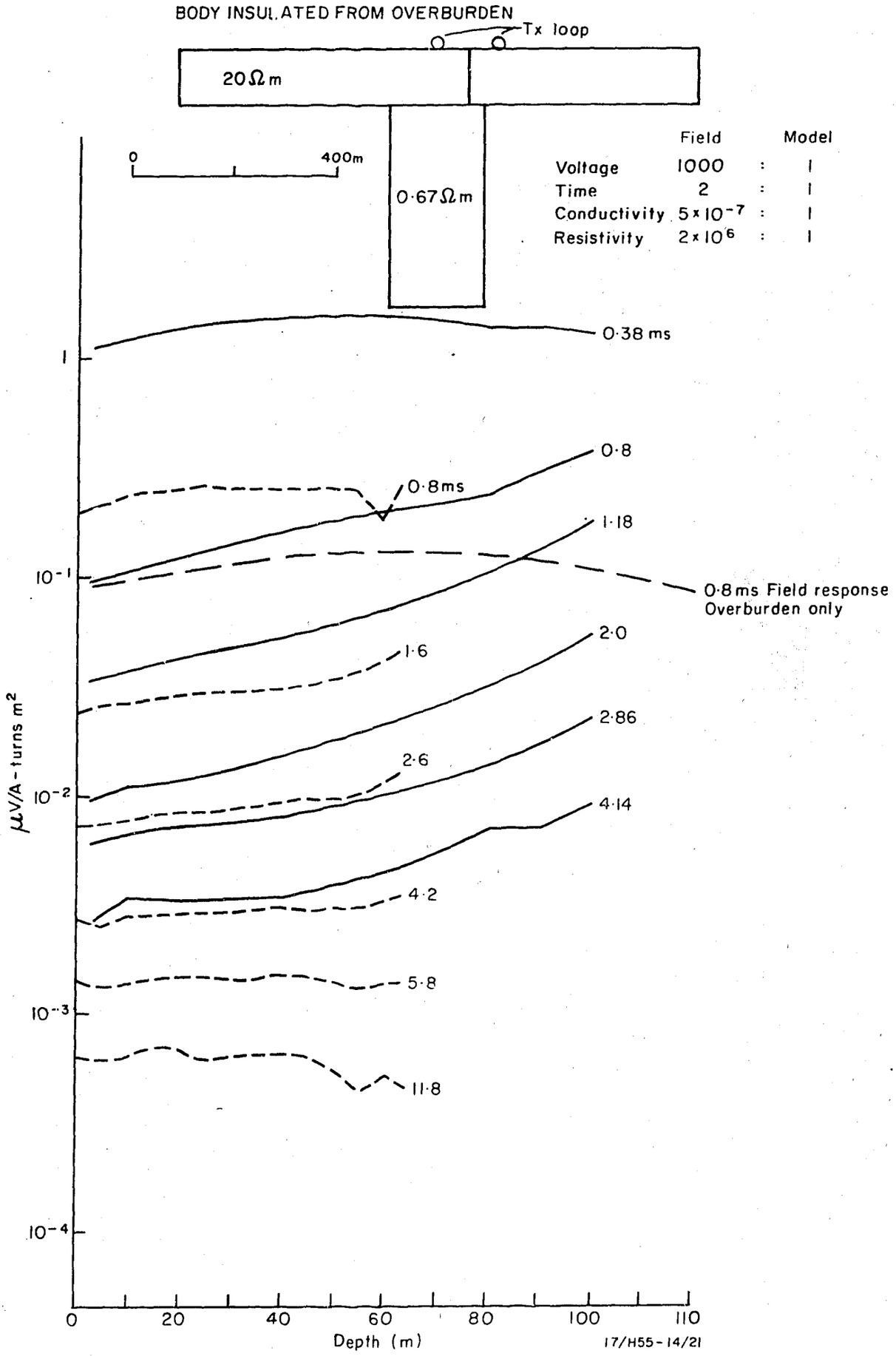

Fig. 21 Curve matching. Model as in Figures 5 and 20 but scale factors are different.

can vary according to the scale factors shown in the diagrams. For each figure the corresponding resistivities of the overburden and orebody are shown.

Figure 21 shows the best curve match at late delay times but a poor match of the levels, and particularly the shape, at 0.8 ms. For this model, in which the overburden is 20 ohm-m, the 0.8 ms model curve increases more steeply than the corresponding field curve. The field curve matches the shape of the 'overburden only' 0.8 ms curve scaled from Figure 3 for a resistivity of 20 ohm-m. The near-surface signal level of the 0.8 ms field curve is about twice that of the 'overburden only' model curve; hence the standard curves of Spies (1978) or the late-time asymptotic formula of Lee & Lewis (1974) imply the bulk resistivity of the overburden is about 13 ohm-m. The inherent assumption that a 20 ohm-m overburden 100 m thick above a resistive halfspace behaves approximately as a 20 ohm-m halfspace at 0.8 ms can be verified from the Raiche & Spies (1981) two-layer master curves. For $\sigma_2/\sigma_1 = 0.001$ and with a loop-radius/layer-thickness ratio of 0.56 and a normalised time of 1.6×10^{-6}, σ_a/σ_1 is 1.0, indicating that the resistive halfspace is not being seen. Thus by matching the curves at late delay times we obtain 0.67 ohm-m for the orebody resistivity, and by matching them at early times and applying a correction we obtain 13 ohm-m for the overburden. Both figures are consistent with Hone's (1980) measurements on core.

This technique for matching the early and late times is an approximation, for while all the contribution to the near-surface measurements at early delay times comes from the overburden only, the response at late delay times comes from both the orebody and overburden. Therefore the curve

shape at late times will be modified by the overburden resistivity. For a more reliable estimate of the overburden and orebody resistivities, the curve matching could be repeated for a model in which the ratio of the overburden to orebody resistivities was 20:1 instead of 30:1.

Figure 20 shows the curves obtained with a 15 ohm-m overburden over a 0.5 ohm-m orebody. The field response at 0.8 ms is intermediate between the 0.51 and 1.1 ms responses and is probably acceptable. Notice that the field response at late delay times falls slightly below the model response, indicating that the resistivity of the model (0.5 ohm-m) needs to be increased.

Borehole near north end of orebody; transmitter loop centred 100 m from borehole

The same curve-matching technique applied to Figure 6 with the Tx loop 100 m north of the borehole gave the best fit for an overburden of 20 ohm-m over a 0.67 ohm-m orebody. The curve fit at 0.8, 1.6, and 2.6 ms was reasonable, but at later delays the fit was poor.

With the Tx loop south and west of the borehole (Figs. 8 and 9 respectively) the model with a 20 ohm-m overburden and a 0.67 ohm-m orebody gave the best curve fit.

Measurements in shaft; transmitter loop over southern part of orebody

A good match between the field curves of Figure 10 and model curves was obtained at 0.8, 1.6 and 2.6 ms down to 110 m with an overburden resistivity of 15 ohm-m and an orebody resistivity of 0.5 ohm-m. Below 110 m the match was poor quantitatively, but there are qualitative features in common (Fig 10): thus, both model and field curves have (1) minimum depressions - between 140 and 170 m at times 2.4, 4.0, and 5.7 ms in the model, and between 110 and 140 m (except for the peak at 120 m, which

Hone & Pik, 1980, attribute to machinery in a drive) at times 1.6, 2.6, 5.8, and 11.8 ms in the field - followed by increases - at 170 m in the model and 140 m in the field; and (2) a highly depressed curve (with negative values) followed by a less depressed curve - at 4.0 and 5.7 ms in the model, and 5.8 and 11.8 ms in the field.

The modelling results show that for depths between 90 and 180 m the signal from the orebody subtracts from the signal from the overburden at all delay times, and confirms Hone & Pik's (1980) category B response from the orebody (negative at all sample times). Notice also that the model response increases at 170 m. A similar increase in the field results was observed by Hone & Pik (1980) at 140 m, and was tentatively attributed to metallic debris at the bottom of the shaft. The model results show there is a real increase in response with depth (although at a greater depth than for the field results) so that the increase observed in the field may also be real.

Measurements in shaft; transmitter loop not over orebody

A good match between the model and field curves of Figure 12 was obtained at 0.8 and 1.6 ms down to 90 m for a 15 ohm-m overburden. Below 90 m and beyond 2.6 ms the field curves were at a higher level than the model curves, owing to the finite resistivity of the host rock in the field compared with the infinite resistivity of the air in the model (i.e., model measurements made in air beneath graphite block). As mentioned earlier, comparison of the model results of Figures 12 and 13 indicates that there is no recognizable response from the orebody for this particular geometry.

7. CONCLUSIONS AND RECOMMENDATIONS

These model studies provide a suite of curves illustrating the TEM response down vertical drillholes through a conductive overburden into a resistive host, and through a conductive overburden overlying a conductive prism approximating the Elura orebody. The results show that at early sample times the overburden alone generates the near-surface response. At depth the response of the orebody is complicated: it may add to or subtract from the overburden response, depending on sample time and the transmitter-receiver-orebody geometry.

Separate tests both with and without the orebody in electrical contact with the overburden indicate, for this simple model, that there is only a marginal increase in the orebody response when it is in contact with the overburden. A recommendation for further work would be to construct a more elaborate model with vertical as well as horizontal boundaries to test the effect of changing their conductivities on the orebody response.

Quantitative comparison of the field and model curves enables the bulk resistivities of the body and overburden to be established by curve-matching techniques based on the basic scaling relationships. This quantitative interpretation requires that the calibration of the model and field probes be known accurately, which in turn leads to the recommendation that the frequency response of the SIROTEM probe should be established by methods similar to those of appendix 2.

The lack of model curves beyond about 4 ms (real time in model) suggests that improvements (such as shielding of 50 Hz or r.f. interference) could be made to the modelling facility to enable measurements at later delay times to be made.

Finally, these model curves are limited. Obviously more elaborate models with a multitude of transmitter and receiver configurations, with vertical and inclined holes, could be modelled.

8. REFERENCES

HONE, I.G., 1980 - Geoelectric properties of the Elura prospect, Cobar, NSW. Bulletin of the Australian Society of Exploration Geophysicists, 11(4), p. 178-183.

HONE, I.G. & PIK, J.P., 1980 - SIROTEM down-hole logging, Elura, Cobar, NSW. Bulletin of the Australian Society of Exploration Geophysicists, 11(4), p. 312-317.

LEE, T. & LEWIS, R., 1974 - Transient EM response of a large loop on a layered ground. Geophysical Prospecting, 22(3), p. 430-444.

NABIGHIAN, M.N., 1979 - Quasi-static transient response of a conducting half-space - an approximate representation. Geophysics, 44(10), p. 1700-1705.

RAICHE, A.P. & SPIES, B.R., 1981 - Coincident loop transient electromagnetic master curves for interpretation of two-layer earths. Geophysics, 46(1), p. 53-64.

SINCLAIR, G., 1948 - Theory of models of electromagnetic systems. Proceedings, Institute of Radio Engineers, 36(11), p. 1364-1370.

SPIES, B.R., 1978 - Interpretation of transient electromagnetic measurements using the apparent conductivity concept. Bureau of Mineral Resources, Australia, Record 1978/85.

SPIES, B.R., 1979 - Scale model studies of a transient electromagnetic prospecting system using an interactive minicomputer. IEEE Transactions on Geoscience Electronics, GE-17(2), p. 25-33.

SPIES, B.R., 1980 - The application of the transient electromagnetic method in Australian conditions - Field examples and model studies. Ph.D. thesis, Macquarie University.

VELIKIN, A.G., & BULGAKOV, Yu. I., 1967 - Transient method of electrical prospecting (one loop version). UNO Conference, Moscow, 1967. Ministry of Geology of the USSR, Moscow.

WARD, S.H., 1967 - The electromagnetic method. In Mining Geophysics, Vol. 2. Society of Exploration Geophysicists, Tulsa, p. 308-315

APPENDIX 1

MODEL PARAMETERS AND LOOP SPECIFICATIONS

PARAMETER	Model		Full scale
Dimension scaling	1	:	2000
Time scaling	1	:	4
Conductivity scaling	1	:	1.0×10^{-6}
Voltage scaling	1	:	500
Deposit:			
Length	87 mm		174 m
Width	52 mm		104 m
Depth below surface	52 mm		104 m
Depth extent	200 mm		400 m
Conductivity	3×10^{6} S/m		3.0 S/m
Overburden:			
Length	500 mm		1000 m
Width	205 mm		410 m
Depth	52 mm		104 m
Conductivity	10^{5} S/m		0.1 S/m
Transmitter loop:			
Mean radius	29.5 mm		59 m
Mean area			1.09×10^{4} m^2
Side of square with equivalent area			105 m
Receiver loop:			
Effective radius	2.98 mm		5.96 m
Effective area			112 m^2
Length of windings	5.0 mm		10 m
Diameter of borehole	10 mm		20 m

Appendix 1 (Contd)

LOOP SPECIFICATIONS

Transmitter:

Number of turns	100
Wire gauge	28 B&S
Mean radius	29.5 mm
Mean height above surface	1.7 mm
Resistance	13.1 ohms
Inductance	1.26 mH
Q at 1 kHz	About 0.6

Receiver:

Number of turns	2000
Wire gauge	42 B&S
Effective radius	2.98 mm
Length of windings	5.0 mm
Resistance	267 ohms
Inductance	14 mH
Q at 1 kHz	About 0.3

APPENDIX 2

COIL CALIBRATIONS

The frequency response of the receiver coil was obtained by placing it in a sinusoidal magnetic field of known amplitude. The output voltage from the coil was measured on a Princeton Applied Research (PAR) model 5204 lock-in analyser to obtain both amplitude and phase relative to the magnetic field. Measurements were made in the frequency range from 10 Hz to 100 kHz and Figure A1 is a plot of:

$$W(j\omega) = V(j\omega)/B(j\omega) \tag{A1}$$

where $W(j\omega)$ is the transfer function relating the input magnetic field $B(j\omega)$ (in teslas) to the output voltage $V(j\omega)$ (in volts).

Figure A2 is a simplified equivalent circuit model for the coil and PAR analyser.

Assuming zero current in the inductor and zero charge on the capacitor at time t = o the output voltage can be written as:

$$V(s) = \frac{Vg(s)}{LC_T s^2 + (RC_T + \frac{L}{R_i})s + 1 + \frac{R}{R_i}} \tag{A2}$$

where

$C_T = C + C_i$ is the sum of the coil capacitance C and the PAR input capacitance Ci,

$V(s) = \mathcal{L}[v(t)]$ the Laplace transform of $v(t)$

$Vg(s) = \mathcal{L}[v(t)]$ the Laplace transform of $vg(t)$

and $\mathcal{L}$ denotes the one-sided Laplace transform defined by

$$F(s) = \mathcal{L}[f(t)] = \int_0^\infty f(t)e^{-st}dt$$

The voltages $v(t)$ and $vg(t)$ are referred to as t domain voltages and $V(s)$ and $Vg(s)$ as s domain voltages.

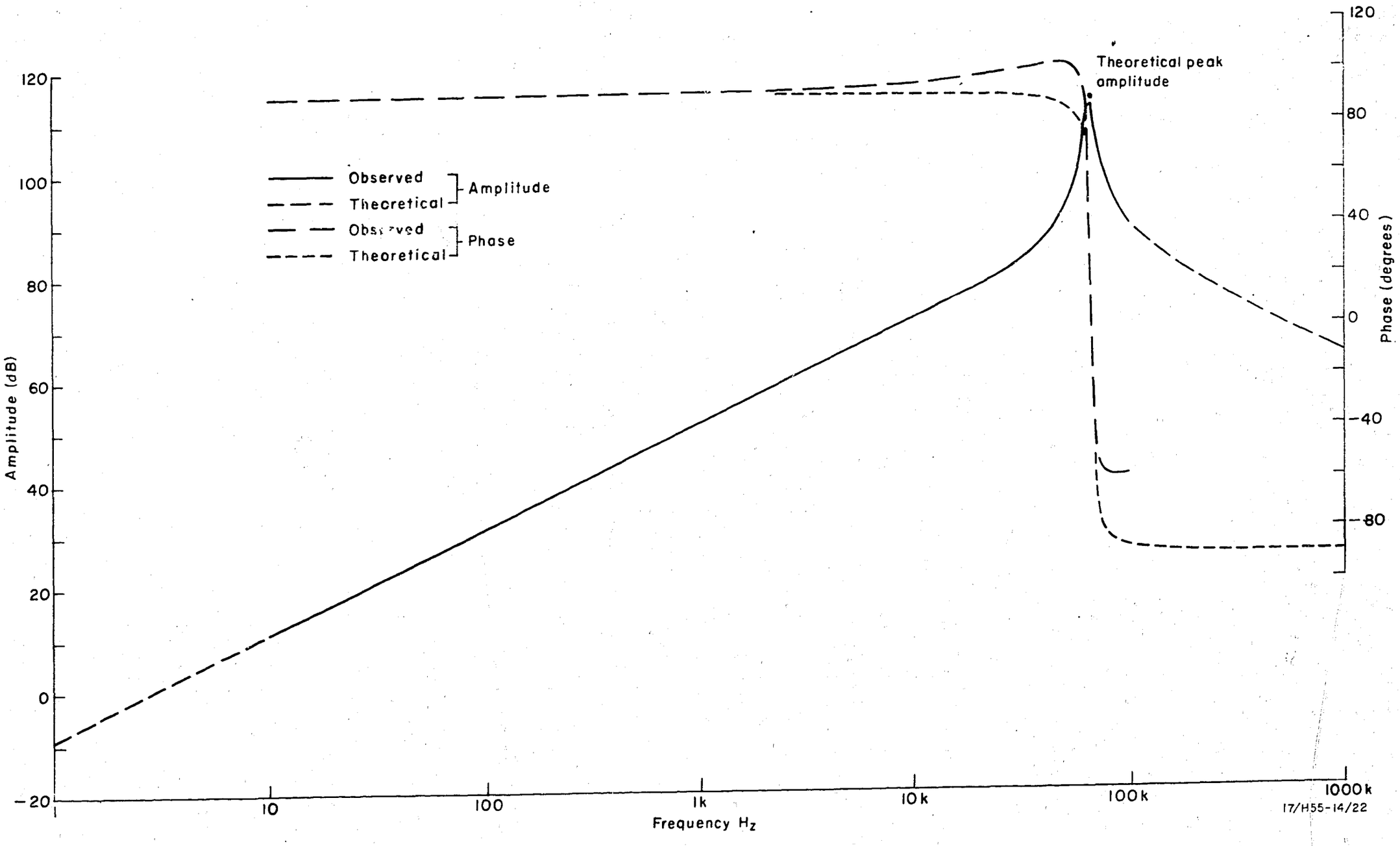

Fig. A1. Theoretical and observed transfer functions relating input magnetic field to output voltage of coil.

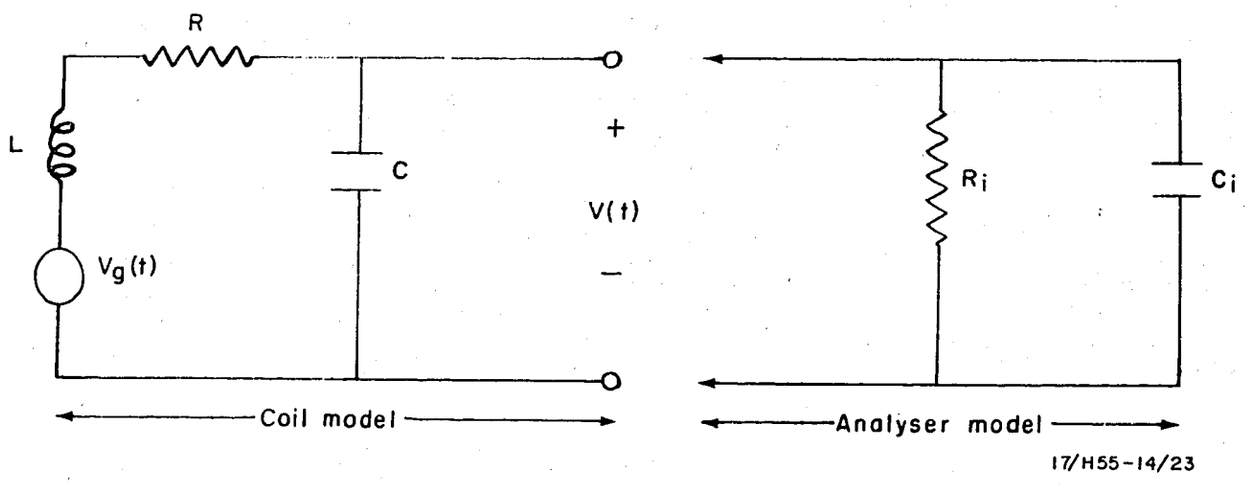

Fig. A2 Simplified equivalent circuit model for receiver coil and PAR analyser.

The expression for $\upsilon g(t)$ is:

$$\upsilon g(t) = NA \frac{d}{dt} b(t) = K\frac{db(t)}{dt} \qquad (A3)$$

where

$\upsilon g(t)$ is the voltage source of the coil model

$b(t)$ is the magnetic flux density

N is the number of turns

A is the area of the coil

K = NA, the turns area product of the coil.

The main objective of the measurements was to establish K, and a secondary objective was to see whether there were any undesirable resonances which might have interfered with the TEM results.

If we take the Laplace transform of equation A3 and assume that $b(t)$ is zero at t = o - i.e., $b(o+) = 0$ - then:

$$Vg(s) = Ks \{B(s) - b(o+)\} = Ks\, B(s) \qquad (A4)$$

If we put this expression for $Vg(s)$ in equation A2 and divide both sides by $B(s)$ we obtain:

$$W(s) \equiv \frac{V(s)}{B(s)} = \frac{Ks}{LC_T s^2 + (RC_T + \frac{L}{R_i})s + 1 + \frac{R}{R_i}} \qquad (A5)$$

which represents the transfer function between the output voltage and the input magnetic field.

For a sinusoidal steady-state input and output, s is replaced by $j\omega$ to yield the transfer function at a particular angular frequency ω - i.e.,

$$W(j\omega) = \frac{V(j\omega)}{B(j\omega)} = \frac{j\omega K}{1 + \frac{R}{R_i} - LC_T\omega^2 + j\omega(RC_T + \frac{L}{R_i})} \qquad (A6)$$

The amplitude of $W(j\omega)$ can be expressed in decibels for convenience of plotting:

$$dB = 20 \log_{10} \left|\frac{V(j\omega)}{B(j\omega)}\right|$$

$$\text{i.e., } dB = 20 \log_{10} K + 20 \log_{10} \omega - 20 \log_{10} \left|1 + \frac{R}{R_i} - LC_T\omega^2 + j\omega\left(RC_T + \frac{L}{R_i}\right)\right| \quad (A7)$$

For the coil, R and L were measured on a bridge and have the values:

$R = 267$ ohms

$L = 14$ mH

From the specifications of the phase lock analyser

$C_i = 25$ pF

$R_i = 10^8$ ohms

The unknowns are K and C of the coil which can be found from the frequency response curve. Now R/R_i and L/R_i are much less than 1, and, for this coil, C is unlikely to be greater than several hundred picofarads; hence at a frequency of 10-100 Hz the amplitude in dB of $W(j\omega)$ simplifies to:

$$dB = 20 \log_{10} K + 20 \log_{10} \omega \quad (A8)$$

because the third term in equation A7 is essentially zero.

So if we plot equation A8 against $\log_{10} \omega$ we will have a curve that rises at 20 dB per decade in its low-frequency range and has the value of $20 \log_{10} K$ for $\omega = 1$ rad s^{-1}. Tge 0 dB point which represents 1 VT^{-1} occurs when $\omega = 1/K$.

The value of K, the turns-area product of the coil, was calculated from the simplified (low-frequency) transfer function:

$$\left|\frac{V(j\omega)}{B(j\omega)}\right| \simeq \omega K$$

whence:

$$K \simeq \frac{1}{\omega} \left|\frac{V(j\omega)}{B(j\omega)}\right| \qquad \text{(A9)}$$

From measurements at 10 Hz:

$$NA = K = \frac{3.51}{2\pi \times 10} = 5.586 \times 10^{-2} \qquad VsT^{-1} \equiv m^2$$

whence:

$$A = \frac{K}{N} = \frac{5.586 \times 10^{-2}}{2000} = 2.793 \times 10^{-5} \ m^2$$

From this the effective radius of the coil can be calculated:

$$r = \frac{\sqrt{2.793 \times 10^{-5}}}{\pi} \ m$$

$$= 2.98 \text{ mm}$$

At high frequencies the final term in equation A7 will be significant. This term is due to the self resonance of the coil, and from its behaviour at and near resonance the value of C_T can be found.

Examination of the measurements from which the transfer function was plotted showed the resonance was very lightly damped with zero phase shift at 67 kHz. For this lightly damped response the resonant frequency is:

$$f_r \simeq \frac{1}{2\pi \sqrt{LC_T}} \qquad \text{(A10)}$$

whence:

$$C_T \simeq \frac{1}{L4\pi^2 f_r^2} = \frac{1}{14 \times 10^{-3} \times 4\pi^2 (67 \times 10^3)^2} = 403 \text{ pF}$$

Now $C = C_T - C_i$

$= 403 - 25 = 378$ pF

Hence all the characteristics of the coil are:

$K = 5.586 \times 10^{-2} VsT^{-1}\ m^2$

$L = 14$ mH

$R = 267$ ohms

$C = 378$ pF

and for the PAR lock-in analyser:

$R_i = 10^8$ ohms

$C_i = 25$ pF

$C_T = 403$ pF

With these values the theoretical transfer function is (using equation A6):

$$W(j\omega) = \frac{V(j\omega)}{B(j\omega)}$$

$$= \frac{j\omega\ 5.586 \times 10^{-2}}{1 + \frac{267}{10^8} - 14 \times 10^{-3} \times 403 \times 10^{-12}\ \omega^2 + j\omega(267 \times 403 \times 10^{-12} + \frac{14 \times 10^{-3}}{10^8})}$$

$$= \frac{j\omega\ 5.586 \times 10^{-2}}{1 - 5.642 \times 10^{-12}\omega^2 + j\omega(1.0774 \times 10^{-7})}$$

Now the denominator corresponds to a pair of complex conjugate poles for which there is a standard form, namely:

$$1 - (\frac{\omega}{\omega_n})^2 + j2\zeta(\frac{\omega}{\omega_n}) \qquad \text{(A11)}$$

where ω_n is the natural (undamped) frequency associated with the inductor and capacitor, and ζ is the damping ratio , which equals one for critical damping.

With the denominator in this form $W(j\omega)$ is:

$$W(j\omega) = \frac{j\omega\ 5.586 \times 10^{-2}}{1 - (\frac{\omega}{4.2100 \times 10^5})^2 + j2(2.2679 \times 10^{-2})\frac{\omega}{4.2100 \times 10^5}} \qquad \text{(A12)}$$

whence $\omega_n = 4.2100 \times 10^5$

i.e., $f_n = \frac{4.2100 \times 10^5}{2\pi} = 67$ kHz

and $\zeta = 2.27 \times 10^{-2}$, i.e., the circuit is underdamped.

Comparison of theoretical and observed curves

The theoretical and observed amplitude and phase curves for $W(j\omega)$ are shown in Figure A1 . The amplitude curves agree well; the maximum discrepancy is at the peak of the resonance where the theoretical curve is 1 dB higher; this could be due to a failure to measure the actual peak of the resonance curve during the observations.

There is a much larger discrepancy between the theoretical and observed phase angles. The cause of this is unknown; it may be that the simple circuit model is inadequate to represent the coil and analyser combination, or it may be due to stray reactance in the circuits monitoring the drive current producing the primary magnetic field.

Step response

These tests have established the value of K, the turns-area product of the coil, and have shown the coil to have a self resonance of 67 kHz. At first sight this high-resonant frequency appears satisfactory. However, further calculations show that the voltage output for a sudden step in the magnetic field strength depends considerably on the input impedance of the circuit to which the coil is connected. In particular, with 10^8 ohms in parallel with 25 pF input impedance of the PAR analyser, the response to a step in the magnetic field is an oscillation at 67 kHz with a decay time constant of 105 μs. With the primary magnetic flux density of about 1.6 mT used in the models, the oscillation would have an amplitude of about 6 V at 0.19 ms (the earliest sample time). This would be a disaster as the model response would be completely swamped. If the input impedance is reduced to 10^4 ohms in parallel with 25 pF, the oscillation is at 64.5 kHz with a decay time constant of 7.48 μs.. With the same primary magnetic flux density the

oscillation would have an amplitude of about 3×10^{-10} V at 0.19 ms, which is quite satisfactory. These figures demonstrate the need for adequate damping of the coil.

Practical aspects

The input impedance of the TEM receiver was unknown, and it varies when the amplifier is gated on and off during the acquisition cycle. Consequently the foregoing theoretical aspects of resonance were not needed during the modelling experiment. In practice the TEM decay waveforms were monitored on the oscilloscope and were free of oscillations at times as short as 0.07 ms, indicating that the coil-amplifier combination was adequately damped. Had this not been so, then the theory would be valuable in deciding what parameters of the combination needed changing to obtain a satisfactory response.

APPENDIX 3

VOLTAGE LEVELS OF MODEL AND FIELD CURVES

Absolute voltage levels of model curves

The output of the TEM modelling facility is the value of the voltage decay at various sample times. The measured voltage is corrected by the computer program for amplifier gain, transmitted current, and turns on the Tx and Rx coils to yield a value in microvolts per amp per turn. This voltage can then be scaled up to that measured in the field by the voltage scaling relationship (equation 3 in section 2).

For an in-loop or down-hole receiver coil it is reasonable to correct this voltage for the effective area of the receiver coil, if we are to make comparisons with other results. Consequently the model results have been normalised to a receiver coil area of one square metre and are expressed in units of microvolts per amp per turn per square metre of receiver coil.

The normalising factor for a length scaling ratio of 2000 and a voltage scaling ratio of 500 (see Appendix 1) can be derived as follows:

effective radius of model Rx coil = 2.98 mm

effective radius of full-scale Rx coil = 5.96 m

effective area of full-scale coil = 111.6 m^2

Let V be the voltage measured in the field (full scale) and Vm the voltage measured in the model in $\mu V\ A^{-1}\ turns^{-1}$. Then:

$$V = 500\ Vm$$

and Vo, the value of V normalised for the Rx coil area, is expressed as:

$$Vo = \frac{V}{111.6} = \frac{500}{111.6} Vm$$

i.e., Vo = 4.48 Vm ($\mu V\ A^{-1}\ turns^{-1}\ m^{-2}$)

which are the values and units used for plotting the model results.

Absolute voltage levels of field curves

The SIROTEM field observations presented by Hone & Pik (1980) were not normalised for the effective area of the down-hole coil. Hone & Pik used a prototype probe to log holes BMR 1 and E36, and the production model to log the shaft. The production probe is similar to the prototype, but has an external diameter of 45 mm instead of 25 mm to reduce capacitative coupling between the coils and the environment. No calibration data are available in terms of the frequency response of these probes. Instead field tests were carried out by CSIRO to compare the TEM response of the probes with the response of square loops of various sizes.

Data supplied by P. Pik (CSIRO, personal communication 1980) show that the TEM decays differ slightly between the two probes when excited by the same 100 x 100 m transmitter loop. The prototype and production probes have the same response from channels 1 (0.4 ms) to 6 (2.6 ms), but the production probe has a larger response from channels 7 (3.4 ms) to 13 (10.2 ms), being 0.5 dB greater at channel 7, and 5 dB greater at channel 13. The effective area calculated for the prototype probe is different when computed from the response to the 100-m-square or the 50-m-square transmitter loop. Comparison of the prototype probe response with the 100-m-square loop response on channels 2 to 8 (0.8 to 2.4 ms) gave an effective area of 5600 m^2 with a standard deviation (SD) of 300 m^2. Comparison of the 50-m-square loop response on channels 2 to 6 gave an effective area of 5100 m^2 with a SD of 350 m^2.

To sum up the effective area of each probe in a single figure, we can say it is about $5300 \pm 600\ m^2$.

For a more accurate estimate of this figure the frequency response of the probes should be measured using a known sinusoidal magnetic field as input. The response of the probe to a known step in the magnetic field could be calculated from the frequency response. The calculations could be checked by measuring the response of the probe to a step in the magnetic field. This in turn approximates the 'self response' of the probe, defined by P. Pik (personal communication 1980) as the 'response produced by the primary field excitation of the receiver leading to a detected signal during the off time measurement'.

The field results of Hone & Pik (1980) have been divided by 5300 (shifted by 3.72 decades on a logarithmic plot) to produce the field data plotted in the figures in units of microvolts per amp per turn per square metre.